

1 **Convoluted nasal passages function as efficient heat exchangers in ankylosaurs**
2 **(Dinosauria: Ornithischia: Thyreophora)**

3

4 Jason M. Bourke^{1#a#b*}, Wm. Ruger Porter^{2 ¶}, Lawrence M. Witmer^{2 ¶}

5 ¹ Department of Biological Sciences, Ohio University Athens, Ohio, USA

6

7 ² Department of Biomedical Sciences, Heritage College of Osteopathic Medicine
8 Ohio University, Athens, Ohio, USA

9

10 #aFormer address: Paleontology Unit, Nature Research Center, North Carolina Museum
11 of Natural Sciences, Raleigh, North Carolina, USA

12

13 #bCurrent address: Department of Basic Sciences, NY Institute of Technology College of
14 Osteopathic Medicine at Arkansas State, Jonesboro, Arkansas

15

16 * Corresponding author

17

18 E-mail: jbourke@nyit.edu (JMB)

19

20 **Abstract**

21 Convoluted nasal passages are an enigmatic hallmark of Ankylosauria. Previous research
22 suggested that these convoluted nasal passages functioned as heat exchangers analogous to the
23 respiratory turbinates of mammals and birds. We tested this hypothesis by performing a
24 computational fluid dynamic analysis on the nasal passages of two ankylosaurs: *Panoplosaurus*
25 *mirus* and *Euoplocephalus tutus*. Our models predicted that *Panoplosaurus* and *Euoplocephalus*
26 would have required 833 and 1568 thermal calories, respectively, to warm a single breath of air
27 by 20°C. Heat recovery during exhalation resulted in energy savings of 65% for *Panoplosaurus*
28 and 84% for *Euoplocephalus*. Our results fell well within the range of values for heat and water
29 savings observed in extant terrestrial amniotes. We further tested alternate airway reconstructions
30 that removed nasal passage convolutions or reduced nasal vestibule length. Our results revealed
31 that the extensive elaboration observed in the nasal vestibules of ankylosaurs was a viable
32 alternative to respiratory turbinates with regards to air conditioning. Of the two dinosaurs tested,
33 *Euoplocephalus* repeatedly exhibited a more efficient nasal passage than *Panoplosaurus*. We
34 suggest that the higher heat loads associated with the larger body mass of *Euoplocephalus*
35 necessitated these more efficient nasal passages. Our findings further indicate that the evolution
36 of complicated airways in dinosaurs may have been driven by the thermal requirements of
37 maintaining cerebral thermal homeostasis.

38

39 Introduction

40 Ankylosaurs were a successful group of ornithischian dinosaurs that had a near global
41 distribution throughout the Cretaceous [1]. Ankylosaurs are best known for their well-armored
42 hides, afforded by extensive osteoderm coverage across the back, sides, and tail, as well as the
43 head [1–3]. In members of Ankylosauridae, these osteoderms continued into the tail where they
44 ended in an expanded and ankylosed tail club. The process behind dermal ossification in
45 ankylosaurs has attracted much interest over the years [4–7]. The mechanism behind the
46 mineralization of soft tissues into a toughened, armored hide appears to have been somatically
47 global, resulting in the mineralization of other epidermal and cartilaginous structures within the
48 body, potentially including the eyelids in *Euoplocephalus tutus* [8]. This tendency to mineralize
49 these soft tissues extended into the nasal passage where Maryńska [9] first observed bony or
50 mineralized structures in the nose of *Pinacosaurus grangeri* that were typically cartilaginous or
51 mucosal in other clades. She interpreted these structures within the nasal cavity of *P. grangeri*
52 and other ankylosaurs as turbinates or conchae [9,10]. Brown [11] was perhaps the first to report
53 the complexity of the nasal cavities of ankylosaurs, pointing to a symmetrical series of air spaces
54 in the snout of *Ankylosaurus magniventris*. Coombs [12] later uncovered a similarly elaborate
55 series of chambers within the nasal cavity of *E. tutus* which he interpreted as an extensive set of
56 paranasal sinuses surrounding the nasal capsule [12–14]. Osmólska [15] suggested a rostral
57 placement of the nasal gland in ankylosaurs based on a sectioned-off recess within the nasal
58 vestibule of *P. grangeri*. Later work challenged this interpretation in favor of an enlarged
59 paranasal sinus system [16] somewhat akin to that described by Coombs for *Euoplocephalus*.
60 Similar observations of paranasal pneumaticity were suggested for other ankylosaurs as well
61 based on the extensive excavations repeatedly uncovered within the nasal cavities of these

62 dinosaurs [14,17–19]. It was only after a detailed computed tomographic (CT) scan of various
63 ankylosaur skulls that it became evident that many of the structures initially interpreted as
64 running parallel to a rather simplistic respiratory passage were in fact parts of bony laminae that
65 braced and separated loops of a remarkably complicated nasal vestibule ([20,21], Fig. 1).

66
67 **Fig 1. Cranium and nasal passage of the two ankylosaur species used for this study.** The
68 nodosaurid, *Panoplosaurus mirus*, ROM 1215 (A) and the ankylosaurid, *Euoplocephalus tutus*,
69 AMNH 5405 (B). Non-modeled nasal passages are shown in greyscale.

70
71 Such a complicated structure begs for a functional explanation. The nasal passage in
72 extant animals offers a variety of functions that amniotes have emphasized in different ways. The
73 nasal passage is a large component of the conducting portion of the respiratory system [22],
74 delivering air from the environment to the lungs. The nasal passage functions in modulating air
75 coming into the lungs by filtering out dust and pathogens. Only a specific portion of the nasal
76 passage functions in odorant detection. The requirements of olfaction run counter to the need to
77 oxygenate the body, requiring regional separation of the nasal passage into a respiratory region
78 and a slower moving olfactory region. The latter region may be expanded into a blind space
79 referred to as the olfactory recess or olfactory chamber in macrosomatic species such as dogs and
80 crocodylians [23,24]. The nasal passage offers a secondary function in phonation, providing
81 resonance to sound waves coming from the pharynx and even acting as a primary means of
82 sound production in certain animals such as saiga antelope and male gharials [25–27]. Lastly, the
83 nasal passage functions to condition respired air by warming and humidifying it upon inspiration
84 and then cooling and drying it on expiration. This conditioning capacity of the nasal passage

85 received extensive study in the latter part of the 20th century [28–33], especially in relation to
86 respiratory turbinates or conchae and their association with the evolution of tachymetabolic
87 endothermy [34–39].

88 Witmer and Ridgely [20] briefly suggested that the elongated airways of ankylosaurs may
89 have functioned in thermoregulation or in vocal resonance. Miyashita et al. [21] expanded on
90 this argument, offering evidence against an olfactory explanation and for either a
91 thermoregulatory or vocal resonance function. Regarding the former, Miyashita et al.
92 [21] described the extensive surface area that a looping nasal passage offers, and coupled this
93 enhanced surface area with evidence for extensive vascular irrigation surrounding the elongated
94 nasal vestibule [20,21]. Such a combination would have resulted in heat transfer from the body
95 to the air regardless of whether or not this was the primary function of the nasal passage [21].
96 However, until now, the thermoregulatory function of these elaborate nasal passages had been
97 inferred solely based on anatomy.

98 We tested the functional hypothesis that the nasal passage in ankylosaurs was an efficient
99 heat exchanger by modeling the airways of two different ankylosaurs; a nodosaurid and an
100 ankylosaurid. To simulate the flow of heat between the nasal passage and the air, we performed a
101 computational fluid dynamic (CFD) analysis. Digital simulation of fluid movement via CFD is
102 routinely performed in the fields of aeronautics [40], automobile engineering [41], and building
103 ventilation [42]. CFD has been successfully applied to biological problems, especially in the
104 realm of biomedicine [43,44], and has been successfully used to simulate airflow in the nasal
105 passages of extant animals [45,46]. Using digital models alleviates the costs associated with
106 physical models, such as choice of material, as well as the costs and complications associated
107 with physical experiments such as flume systems and wind tunnels. Digital simulation of fluid

108 movement via CFD provides a cost-effective means of testing multiple flow speeds, which is
109 difficult to obtain *in vivo* for extant animals and impossible for long-extinct taxa. An added
110 benefit of digital simulations is that they provide the opportunity to digitally manipulate the nasal
111 passages which allowed us to test the preserved airways against soft-tissue-corrected versions.
112 This approach allowed us to perform secondary analyses that tested the effects of length and
113 convolutions using digitally manipulated airways that were either shortened or straightened (Fig.
114 2). In addition to general airflow characteristics, we modeled the heat-transfer potential within
115 the nasal passages of these two dinosaurs. General energetic costs associated with heating and
116 humidifying the airway were calculated based on equations from modern birds. Results were
117 compared to each other and to previously published results on extant animals to determine if the
118 effectiveness of the nasal passage in ankylosaurs was within the range observed in extant
119 animals. We were particularly interested in seeing how well a non-turbinate filled nasal passage
120 would compare to the extensive, turbinate-filled noses of most extant mammals and birds.

121 To ensure that our methods were sound, we performed a validation experiment using a
122 digitized pigeon airway and compared our results to previously published results in the literature.

123 **Institutional Abbreviations**

124 AMNH, American Museum of Natural History, New York, USA; CMN, Canadian
125 Museum of Nature, Ottawa, CA; ROM, Royal Ontario Museum, Ontario, CA; ZPAL, Institute of
126 Paleobiology (Zakład Paleobiologii) of the Polish Academy of Sciences, Warsaw, PL.

127 **Anatomical Abbreviations**

128 a nas, apertura nasalis; air, airway; ant sin, antorbital sinus; bone, bone of nasal cavity; bna, bony
129 narial aperture; cap, cartilaginous nasal capsule; ch, choana; ch f, choanal fossa; ch fd, choanal

130 fold; ch fp, choanal flap; ch g, choanal groove; cnp, cavum nasi proprium; co, concha; ept,
131 ectopterygoid; f ex, fenestra exochoanalis; j, jugal; lam, lamina transversa; max, maxilla; mnca,
132 median nasal caputegulum; mu, mucosa; nar, naris; ns, nasal; nvas, neurovasculature; olf,
133 olfactory recess; olf turb, olfactory turbinate; p2, secondary palate; pal, palatine; pmax,
134 premaxilla; pt, pterygoid; q, quadrate; tr, tracheal extension; turb, turbinate; v, vomer; vest, nasal
135 vestibule.

136
137 **Fig. 2. Summary of models analyzed in this study.** *Panoplosaurus* (A,B,E,F) and
138 *Euoplocephalus* (C,D,G,H) nasal passages were modeled as preserved, or bony-bounded (A,C),
139 with soft-tissue correction (B,D), simplified (E,G) or with all convolutions removed (F,H). See
140 Methods section for specifics for each model.

141

142 **Results**

143 **Validation test**

144 During inspiration, the nasal passage of our pigeon model warmed incoming air by 22°C,
145 bringing the air field close to body temperature by the time it reached the throat. Subsequently, a
146 22°C drop in temperature was applied to the nasal walls of the expiration model. To test heat
147 transfer during expiration, air within the trachea was set to a temperature of 38°C, reflecting
148 empirically obtained data on tracheal temperature in pigeons during expiration [38]. The
149 converged expiration model revealed an air temperature drop from 38°C to 21.6°C at the nostril
150 (Fig. 3). This 16.4°C drop in temperature was within the range of values obtained by Geist ([38],

151 Table 1), suggesting that our methodology was producing results similar to *in vivo* animal
152 experiments.

153 **Table 1. Comparison of values for heat transfer in domestic pigeons (*Columba livia*)**
154 **between experimental data [38] and simulation (this study)**

Study	Mass (g)	Body temp (°C)	Ambient air (°C)	Oral temp (°C)	Exhaled temp (°C)
38	319 (+/- 45.2)	40.7	15	38.2 +/- 0.5	21.4 +/- 0.5
This study	455	40.7	15	38	21.6

155

156 **Fig 3. Airflow and heat transfer within the left nasal passage of a pigeon (*Columba livia*).**

157 (A) Airway was segmented out from the head and (B) converted into a volumetric mesh for CFD
158 analysis following methods in the text. (C) Heat transfer simulation was performed under an
159 inspiratory flow condition and data from that simulation was used to inform (D) the expiratory
160 flow conditions. Artificial laryngotracheal extension was omitted in C & D as no data from that
161 region was used.

162 *Panoplosaurus mirus*

163 **Bony-Bounded (BB) airway (Fig 2A)**

164 Under the high flow rate condition, the BB airway was able to successfully increase
165 inspired air temperature by 18.2°C (Fig. 4). Most (93%) of this heating took place inside the
166 elongate nasal vestibule. The relative humidity of the inspired air reached saturation prior to
167 entering the cavum nasi proprium (CNP). The larger volume of the nasal passage produced
168 slower-moving air with a fair amount of vorticity present inside the CNP. Inspired air left the
169 choana at 33.2°C. During expiration, air left the nostrils at 22.7°C. Under the low flow rate
170 condition, the BB nasal passage was able to warm inspired air to 18.6°C, with 92% of airway
171 heating taking place within the nasal vestibule. Moisture content of the air achieved saturation

172 earlier than in the high flow condition. The low flow rate condition exhibited more laminar
173 airflow compared to the more turbulent high flow condition. On expiration, the low flow
174 condition BB airway reduced air temperature down to 20.5°C prior to exiting the nostrils.

175

176 **Fig 4 Heat flow within the BB nasal passage of *Panoplosaurus mirus* (ROM 1215) during**
177 **inspiration under both high (left) and low (right) flow scenarios.** Numbers of dotted lines
178 indicate cross-section numbers. Cross sections were taken at equivalent locations on both
179 models.

180

181 **Soft-Tissue (ST) airway (Fig. 2B)**

182 Under the high flow rate condition, the nasal passage of *Panoplosaurus* was able to heat
183 inspired air by 17.9°C. The convoluted nasal vestibule was responsible for the majority of the
184 heat transfer (94%, Fig. 5). Similarly, relative humidity of the inspired air had reached saturation
185 prior to entering the CNP. Air left the choana at 32.9°C. Vortices were observed in the first
186 portion of the nasal vestibule (rostral loop of Witmer & Ridgely [20]) as well as the CNP near
187 the olfactory recess. Upon expiration, air entered the choana at 35°C and left the nostril at
188 21.6°C. Expiratory flow was more laminar than inspiratory flow, with very few vortices
189 observed throughout the nasal passage. Under the low flow rate condition, the nasal passage of
190 *Panoplosaurus* warmed inspired air by 19.3°C. Similar to the high flow rate condition, most of
191 the heat transfer (89%), and all of the moisture transfer, occurred within the convoluted nasal
192 vestibule (Fig. 5). The CNP contributed more to airway heating under this scenario than under
193 the high flow rate condition. Similar vortices were observed in the low flow rate condition as in

194 the high flow rate condition (Fig. 5). On expiration, air in the low flow rate condition left the
195 nostril at 19.5°C.

196

197 **Fig 5. Heat flow within the soft-tissue corrected nasal passage of *Panoplosaurus mirus***
198 **(ROM 1215) during inspiration under both high (left) and low (right) flow scenarios.**

199 Numbers of dotted lines indicate cross-section numbers. Cross sections were taken at equivalent
200 locations on both models.

201

202 **Basic airway (Fig 2E)**

203 The basic airway consisted of a plesiomorphic, truncated nasal vestibule that extended in
204 a straight line from the nostril to the opening of the CNP (Fig. 6). The total length of this
205 simplified nasal vestibule was 200 mm. This reduced the length of the original 440 mm nasal
206 vestibule by 55%. As this basic airway was strictly a hypothetical construct, we only ran the
207 model under the more conservative, Reversed-Reynolds condition (see Methods). The lower
208 flow rate associated with this condition provided the shorter airway with the best opportunity to
209 transfer heat from the nasal passage. Despite this lower flow rate, the basic airway had difficulty
210 transferring a substantial amount of heat from the nasal passage to the inspired air. On the outset,
211 this difficulty was not entirely clear as the entire nasal passage was able to warm inspired air by
212 17.6°C (Fig. 6) and achieve moisture saturation. However, only 63% of the heat exchange took
213 place inside the truncated nasal vestibule. This was evident upon examining the temperature
214 distribution through the nasal passage (Fig. 6). Sagittal cross sections of the nasal passage
215 revealed a consistent, low-temperature central stream of air that traveled through the nasal
216 vestibule and remained largely unchanged by the surrounding nasal mucosa. This resulted in a

217 cool stream of air entering the CNP (Fig. 6A). Placing a greater emphasis on the CNP to heat the
218 remainder of the air field proved detrimental to heat savings as the final expired air temperature
219 at the nostril was a relatively high 26.5°C (Fig. 6B).

220

221 **Fig 6. Airflow through the basic airway of *Panoplosaurus mirus* (ROM 1215).** (A) Left
222 lateral view of nasal passage with air streams showing general air field pattern. Airway is color-
223 coded for temperature (hotter colors = hotter temperatures. *Inset*: Sagittal cross section of the
224 nasal vestibule and CNP showing central stream of cool air passing through the nasal vestibule.
225 (B) Temperature at the nostril during expiration for the basic airway and the ST airway.

226

227 **Straightened airway (Fig 2F)**

228 Removing the curvature from the lengthened nasal vestibule ameliorated the vorticity
229 observed in the BB and ST airway models. Under the low flow condition, the straightened
230 airway warmed air by 18.3°C prior to leaving through the choana (Fig. 7). 78% of that heating
231 occurred in the much-elongated nasal vestibule. Similarly, the elongated vestibule was able to
232 completely saturate the inspired air field prior to reaching the CNP, as in the ST and BB airway
233 models. On expiration, the nasal passage reduced the heat of the expired air by 11°C, resulting in
234 expired air leaving the nostril at 23.9°C.

235

236 **Fig 7. Airflow comparison between the straightened airway and the ST airway in**
237 ***Panoplosaurus mirus* (ROM 1215).** (A) Dorsal view of the skull of *P. mirus* with left ST airway
238 in situ. (B) Dorsal view of the straightened airway with flow lines in place. Airflow lines are

239 color-coded for temperature (hotter colors = hotter temperatures). *Inset*: Magnified region of
240 nasal vestibule showing evenly spaced, straight flow lines. (C) Dorsal view of the ST airway
241 under the low flow scenario. Vorticity is observable throughout the nasal vestibule. Note: ST
242 airway in C is not to scale with straightened airway B.

243 *Euoplocephalus tutus*

244 **Bony-Bounded (BB) airway (Fig2C)**

245 Under the high flow rate condition, the BB airway was able to warm inspired air by
246 18.8°C, with 82% of that heating taking place within the confines of the nasal vestibule (Fig. 8).
247 Relative humidity of inspired air reached saturation by the time it reached the caudal loop of the
248 nasal vestibule. Vorticity was evident in most of the bends of the nasal vestibule as well as inside
249 the spacious CNP. On expiration, the nasal passage reduced the expired air temperature by
250 13.9°C, resulting in air leaving the nostrils at 21.1°C. Under the low flow rate condition, the BB
251 airway warmed inspired air by 18.8°C, with 88% of the heat exchange and 100% of the moisture
252 exchange occurring inside the convoluted nasal vestibule (Fig. 8). Despite a lower flow rate,
253 standing vortices along the curves of the nasal vestibule were still present. On expiration at this
254 low flow rate, the nasal passage was able to reduce the temperature of expired air by 15.6°C,
255 resulting in air leaving the nostrils at 19.4°C.

256

257 **Fig 8. Heat flow within the BB nasal passage of *Euoplocephalus tutus* (AMNH 5405) during**
258 **inspiration under both high (left) and low (right) flow scenarios.** Numbers of dotted lines
259 indicate cross-section numbers. Cross sections were taken at equivalent locations on both
260 models.

261 **Soft-Tissue (ST) airway (Fig 2D)**

262 Under the high flow rate condition for *Euoplocephalus*, the nasal passage warmed air by
263 19.7°C with essentially all that heat transfer (97%) occurring in the convoluted nasal vestibule
264 (Fig. 9). Air field relative humidity reached saturation earlier in the nasal vestibule of the ST
265 airway than the BB airway. Extensive vorticity was observed throughout the nasal passage.
266 These vortices were often concentrated around the multiple convolutions within the nasal
267 passage. Upon expiration, air entered the choana at 35°C and exited the nostril at 17.3°C. As
268 with *Panoplosaurus*, there were fewer vortices upon expiration than inspiration. Under the low
269 flow rate condition for *Euoplocephalus* the air field showed complete warming from ambient
270 (15°C) to body temperature (35°C) with almost all of the heat transfer occurring within the
271 convoluted nasal vestibule (99%). Relative humidity of the air field reached saturation slightly
272 earlier within the nasal vestibule. Similar flow patterns to the high flow condition were observed
273 under the low flow rate condition (Fig. 9). During expiration, air left the nostril at 15.9°C, which
274 was just above ambient temperature.

275

276 **Fig 9. Heat flow within the soft-tissue corrected nasal passage of *Euoplocephalus tutus***
277 **(AMNH 5405) during inspiration under both high (left) and low (right) flow scenarios.**

278 Numbers of dotted lines indicate cross-section numbers. Cross sections were taken at equivalent
279 locations on both models.

280

281 **Basic airway (Fig 2G)**

282 As with *Panoplosaurus*, the basic airway for *Euoplocephalus* consisted of a simple nasal
283 vestibule that extended in a straight line from the nostril to the CNP (Fig. 10). The total length of
284 this simplified nasal vestibule was 162.14 mm, which was an 80% reduction in length from the
285 original 808.74 mm nasal vestibule. As with the basic *Panoplosaurus* airway model, we ran this
286 model under our most conservative, Reversed-Reynolds flow estimate. Under this low flow
287 condition, the basic airway of *Euoplocephalus* warmed inspired air by 15.3°C. This initially
288 appeared impressive. However, as with our *Panoplosaurus* model, closer examination of the
289 nasal passage revealed distinct differences between this basic airway and the ST airway. The
290 basic airway of *Euoplocephalus* had a fairly ineffective nasal vestibule. The nasal vestibule
291 provided only 45% of the heat to the air field, resulting in a steady stream of cool air moving
292 through the nasal vestibule and into the CNP (Fig. 10). Air field relative humidity still reached
293 saturation, but only after passing into the CNP. Similar to the basic airway of *Panoplosaurus*,
294 this reliance on the CNP to deliver heat to the inspired air field had direct consequences for the
295 nasal passage during expiration, where the nasal passage was only capable of reducing airway
296 temperature by 4.7°C. The resulting expired air left the nasal passage at just 5°C below body
297 temperature (30.3°C).

298

299 **Fig 10. Airflow through the basic airway of *Euoplocephalus tutus* (AMNH 5405).** (A) Left
300 lateral view of basic airway showing airflow. Streamlines are color-coded for heat (hotter colors
301 = hotter temperatures). *Inset*: Sagittal cross section of airway showing persistent stream of cool
302 air traversing the nasal vestibule and interacting with the CNP. (B) Temperature at the nostril
303 during expiration for the basic airway and the ST airway.

304

305 **Straightened airway (Fig 2H)**

306 The removal of nasal vestibule curvature resulted in vortex-free, laminar air traversing
307 the nasal vestibule (Fig. 11). Under the low flow condition, the straightened airway of
308 *Euoplocephalus* was able to increase the temperature of inspired air by 19.3°C, with 89% of that
309 heating occurring in the nasal vestibule. Water saturation of the inspired air occurred well within
310 the nasal vestibule. On expiration, the straightened airway reduced the temperature of the expired
311 air by 12.2°C, resulting in air leaving the nostrils at 22.8°C.

312

313 **Fig 11. Airflow comparison between the straightened airway and the ST airway in**

314 *Euoplocephalus tutus* (AMNH 5405). (A) Dorsal view of the skull of *E. tutus* with the left ST
315 airway in situ. (B) Dorsal view of the straightened airway with flow lines in place. Airflow lines
316 are color-coded for temperature (hotter colors = hotter temperatures). *Inset*: Magnified region of
317 nasal vestibule showing evenly spaced, straight flow lines. (C) Dorsal view of the ST airway
318 under the low flow scenario showing the presence of vorticity throughout the nasal vestibule.
319 Note: ST airway in C is not to scale with straightened airway B.

320

321 **Energetic costs vs. savings of air conditioning**

322 The estimated volumes of air that would have been inspired during one breath for
323 *Panoplosaurus* and *Euoplocephalus* were 34 and 64 liters, respectively (Table 2). The energetic
324 cost of heating these volumes of air was 833 thermal calories for *Panoplosaurus* and 1568

325 thermal calories for *Euoplocephalus*. Calculated energy savings for *Panoplosaurus* and
 326 *Euoplocephalus* based on the expired air temperatures are presented in Tables 3 and 4.

327

328 **Table 2. Energetic cost of heating one bolus of air by 20°C at 50% relative humidity for**
 329 *Panoplosaurus mirus* and *Euoplocephalus tutus*

Taxon	Tidal volume (ml)	Mass of air (g)	Cost of heating air 20°C (cal)	Latent heat of evaporation (cal)	Total energy cost (cal)
<i>P. mirus</i>	34000	39	187	646	833
<i>E. tutus</i>	64000	73	350	1218	1568

330

331 **Table 3. Energy savings from reducing expired air temperature in all airway models for**
 332 *Panoplosaurus mirus*

Model	Expired temp (°C)	Heat savings (cal)	Latent heat of condensation (cal)	Total energy recovered (cal)
BB airway (high)	22.67	115	392	507
BB airway (low)	20.46	136	441	577
ST airway (high)	21.57	126	419	545
ST airway (low)	19.48	145	460	605
Basic airway	26.5	79.5	294	374
Straightened airway	23.93	103	363	466

333

334 **Table 4. Energy savings from reducing expired air temperature in all airway models for**
 335 *Euoplocephalus tutus*

Model	Expired temp (°C)	Heat savings (cal)	Latent heat of condensation (cal)	Total energy recovered (cal)
BB airway (high)	21.11	244	803	1047
BB airway (low)	19.42	274	868	1142
ST airway (high)	17.34	311	934	1245
ST airway (low)	15.87	337	980	1317
Basic airway	30.3	83	335	418
Straightened airway	22.77	214	738	952

336

337 **Discussion**

338 **Critique of methods**

339 **Nostril placement**

340 The lack of soft-tissue preservation around the nostril makes it difficult to determine just
341 how large the nostril would have been in life, as well as its orientation (lateral vs. terminal). The
342 shape of the nostril has been implicated in directing the air field to parts of the nose in rats and
343 dogs [47,48]. Sauropsids show less nostril mobility than mammals, suggesting that nostril shape
344 is less important for sauropsid nasal airflow dynamics. Nonetheless, the lack of information on
345 nostril shape in extinct animals does limit our knowledge of air field shape in this region of the
346 nose (see Methods). Fortunately, prior studies on how nostril shape alters nasal fluid dynamics
347 indicate that the effects of the nostril on the air field are of limited areal extent, with nasal flow
348 patterns remaining unaffected by nostril placement throughout most of the nasal passage [47].

349 **Energy calculations based on V_T**

350 The caloric energy expenditures and savings that were calculated for each ankylosaur are
351 contingent on our estimates of tidal volume respired during one breath. This tidal volume came
352 from the mass-dependent equations of Frappell et al. [49]. However, as we indicated with flow
353 rate (see Methods), the masses of our two ankylosaurs were substantially greater than those for
354 any of the birds in the dataset of Frappell et al. [49]. Furthermore, the body plan of ankylosaurs
355 is vastly different from their avian relatives, which may negate the use of a tidal volume equation
356 based on birds. However, data from Frappell et al. [49] and Farmer [50] indicate that the tidal
357 volume of archosaurs may be conserved. The mass-dependent equations for tidal volume in birds
358 and crocodylians [49,50] differ only in their coefficients, with that difference being a fairly

359 negligible 0.4. If we used the equation for crocodylian tidal volume instead, it would have
 360 increased tidal volume by 1.5–3%, resulting in a 1–3% increase in caloric costs. This fairly small
 361 increase in caloric costs would not have changed the comparative results between these two taxa,
 362 nor their comparisons to extant animals.

363 **Body temperature estimates**

364 Our study specimens were both given a core body temperature of 35°C based on an
 365 approximate average taken from our survey of extant, large terrestrial tetrapods (Table 5).
 366 Although there has been promising work in paleothermometry using clumped isotopes [51,52],
 367 this technique has yet to be applied to any ankylosaur taxon. Thus, it is likely that our estimated
 368 body temperature for these two dinosaurs is either too high or too low compared to their actual
 369 body temperatures. Despite the arbitrariness of our temperature designation, changing the body
 370 temperature to something higher or lower would have only affected the steepness of the heat
 371 transfer gradient. Our comparative results would remain the same, with *Euoplocephalus*
 372 consistently outperforming *Panoplosaurus*, and the nasal passages of both taxa outperforming
 373 their simplified and straightened airway morphologies.

374
 375 **Table 5. Core body temperatures recorded for a variety of large, terrestrial amniotes**

Taxon	Body Temperature (°C)	Reference
African elephant (<i>Loxodonta Africana</i>)	36.2–36.6	[53,54]
Asian elephant (<i>Elephas maximus</i>)	35.7–36.8	[55,56]
Black rhinoceros (<i>Diceros bicornis</i>)	31.8–41.9	[57,58]
White rhinoceros (<i>Ceratotherium simum</i>)	33.6–37.5	[59,60]
Masai giraffe (<i>Giraffa camelopardalis</i>)	35.7–39.1	[33,61,62]

Grizzly bear (<i>Ursus arctos</i>)	36.5–38.5	[63]
Emu (<i>Dromaius novaehollandiae</i>)	37.4–39.2	[64,65]
Ostrich (<i>Struthio camelus</i>)	38.0–40.2	[65,66]
Galapagos tortoise (<i>Chelonoidis nigra</i>)	28–31	[67]
Komodo dragon (<i>Varanus komodoensis</i>)	36–40	[68]

376

377 **Heat transfer efficiency in ankylosaur nasal passages**

378 Both ankylosaur nasal passages revealed a substantial capacity to modify the conditions
379 of the air within, indicating that the highly convoluted nasal vestibules of these taxa were
380 efficient heat exchangers. The ST airways under the low flow rate condition, recouped the most
381 energy for both dinosaur taxa (73% and 84% for *Panoplosaurus* and *Euoplocephalus*,
382 respectively). This version of the nasal passage was meant to most closely represent what the
383 original nasal passage would have been like in life. In contrast, the nasal passages as they were
384 preserved in the fossils (i.e., the BB airways) and placed under the same low flow rate
385 conditions, were not able to recoup as much heat energy (69% and 73% of inspiratory cost for
386 *Panoplosaurus* and *Euoplocephalus*, respectively). Despite the remarkably well-preserved nasal
387 passages of both dinosaurs, accounting for soft tissue still resulted in noticeable differences in
388 heat transfer efficiency. Comparing the energy savings calculated for the ST airways of
389 *Panoplosaurus* and *Euoplocephalus* (Fig 2B,D) to experimentally obtained energy and water
390 recovery values for extant amniotes, we found both dinosaurs had energy and water recovery
391 values that were on par with many extant animals (Fig. 12).

392 **Fig 12. Heat and water savings calculated for the most efficient airway models of**
393 ***Panoplosaurus mirus* and *Euoplocephalus tutus* vs. various extant animals.** Note that
394 variations in experimental protocol means that, although these results are comparable, they
395 should not be viewed as fully equivalent. See Methods for details on graph calculation and
396 references for extant data.

397

398 As predicted, airflow rate did have a noticeable effect on heat transfer efficiency, with
399 lower flow rates resulting in more effective heat transfer (11–14% and 6–9% greater efficiency
400 for *Panoplosaurus* and *Euoplocephalus*, respectively; Fig. 13). These results agree with previous
401 measurements and simulations [69,70] that indicate flow rate is one of the most important
402 contributing factors affecting heat transfer between air and the nasal passage.

403

404 **Fig 13. Heat and water savings between all nasal airway models for *Panoplosaurus mirus***
405 **(top) and *Euoplocephalus tutus* (bottom).** Models are organized from greatest savings to least
406 in both graphs. Abbreviations: ST low, soft-tissue low flow rate; ST high, soft-tissue high flow
407 rate; BB low, bony-bounded low flow rate; BB high, bony-bounded high flow rate; Straight,
408 straightened airway; basic, basic airway.

409

410 That the heat transfer efficiency of the dinosaur nasal passages was a result of their great
411 length was made evident upon comparison with the artificially shortened basic airways
412 (Figs.2E,G, 6, 10, 13). These basic airways represented a minimalistic trek of the nasal vestibule
413 from the nostril to the CNP. Achieving this ultra-conservative anatomical shape required
414 excising most of the preserved nasal vestibule (55% and 80% of the nasal vestibule length in

415 *Panoplosaurus* and *Euoplocephalus*, respectively). These truncated nasal vestibules offered a
416 much-reduced surface area for heat and moisture to transfer from the respired air to the nasal
417 mucosa (Figs. 6, 10). Although the CNP did offer a sizeable heat transfer capacity during
418 inspiration, this appears to be due to vorticity within the CNP during inspiration. During
419 expiration, expired air traversed the CNP differently from inspiration. Vorticity was not present
420 and heat transfer through the CNP was minimized, requiring the nasal vestibule to handle the
421 bulk of heat transfer. As such, the basic airways showed extremely reduced heat recovery
422 abilities (62–32% of the respective ST airway heat recovery for *Panoplosaurus* and
423 *Euoplocephalus*, Tables 3, 4, Fig. 13). These results strongly suggest that airway elaboration
424 offers a strong thermoregulatory benefit.

425 Maintaining the length but removing curvature (convolutions) from the nasal vestibule
426 (Fig 2F,H) resulted in a negative effect on heat and water recovery ability (Fig. 13), albeit not as
427 prominent as the basic airway. When compared to the low flow rate ST airways, curvature
428 removal resulted in a 23% drop in heat transfer efficiency for *Panoplosaurus* and a 28% drop in
429 heat transfer efficiency for *Euoplocephalus*. The removal of airway curvature also removed the
430 presence of standing vortices in the nasal vestibules of both taxa (Figs. 7, 11), which likely
431 explains the reduced heat transfer. As fluid flows within an object (e.g., air in the nasal passage)
432 the portions of the flow field closest to the object's surface tend to stick to that surface, imparting
433 drag on the fluid as a whole [71]. As streamlines move farther and farther from these surfaces,
434 the sheer imparted by wall drag gets minimized, resulting in fluid at the center of the flow field
435 moving at the highest velocities and producing the classic fluid dynamic parabolic profile [71].
436 Since fluids at the fluid-surface boundary are essentially static, they create a boundary layer that
437 acts as a barrier to diffusion. For laminar flowing fluids, this boundary layer can be fairly thick.

438 Thus, effective heat transfer through laminar fluids requires a reduction in this boundary layer
439 size [71]. One way to reduce this boundary layer effect is by placing sharp turns and contortions
440 within the nasal passage to break up the boundary layer, allowing cooler air to come into closer
441 contact with the surrounding mucosa. The presence of standing vortices at multiple curves within
442 the nasal passage of both *Panoplosaurus* and *Euoplocephalus* (Figs. 7C, 11C) revealed multiple
443 regions where that boundary layer was broken up. Further, the presence of vortices acts to slow
444 down the passage of the air molecules through the nasal passage, providing more time for air to
445 reach thermal equilibrium with the body. By coiling the nasal passage within the skull,
446 ankylosaurs were able to take advantage of the extra surface area for air to interact with the
447 mucosa. This surface area, coupled with the adjacent location of large nasal vasculature ([20,72]
448 Fig. 14) and boundary-layer-breaking effects produced by forcing the air field to radically alter
449 direction as it moved through the nasal vestibule, resulted in these nasal passages acting as very
450 effective air conditioners.

451

452 **Fig 14. Vascular reconstruction of the venous pathway in the left oronasal apparatus of**

453 *Euoplocephalus* (AMNH 5405). Venous reconstruction followed the methods of Porter [72].

454 Red highlighted veins indicate main channels of heat transfer from the oronasal apparatus to the
455 brain.

456

457 The ST airway reconstructions (Fig 2B,D), under the low flow rate conditions, produced
458 the highest water savings (69% and 79% for *Panoplosaurus* and *Euoplocephalus*), whereas the
459 truncated, basic airways were the least effective (44% and 27%) at water reclamation. Our data

460 suggest that the nasal passages in both ankylosaurs could have functioned effectively as water
461 reclaimers as well as air conditioners.

462 **Heat transfer in *Panoplosaurus* vs. *Euoplocephalus***

463 A consistent trend observed throughout this study was the greater heat transfer efficiency
464 in the nasal passage of *Euoplocephalus* (Table 4, Fig. 13 bottom) as compared to *Panoplosaurus*
465 (Table 3, Fig. 13 top). Under both high and low flow rate conditions, both the BB and ST
466 airways of *Euoplocephalus* (Fig 2C,D) were able to bring inspired air closer to simulated body
467 temperature than the respective airway models of *Panoplosaurus* (Fig 2A,B). Upon expiration,
468 the ST nasal passage of *Euoplocephalus* was able to lower air temperatures 3.6–4.2°C lower than
469 air temperatures in the ST-corrected nasal passage of *Panoplosaurus* (Figs. 4–5, 8–9). This
470 translated into a 15–22% greater energy savings and a 14–19% greater water recovery. The more
471 elaborately convoluted nasal vestibule in *Euoplocephalus* compared to *Panoplosaurus* ([20],
472 Figs. 15–18) was likely responsible for these greater energy savings despite the larger flow rates
473 and tidal volumes. The nasal vestibule played the largest role in air conditioning for both models.
474 These results indicate that *Euoplocephalus* had a more effective nasal passage than
475 *Panoplosaurus* in relation to heat transfer. The evolutionary pressures behind these different
476 performances are difficult to decipher.

477 Both ankylosaurs are known from the same stratigraphic level of the Dinosaur Park
478 Formation [73], indicating that they were sympatric. As such, it is unlikely that gross
479 environmental factors were responsible for the more elaborate nasal passages of *Euoplocephalus*.
480 It is possible that the more elaborate nasal passage in *Euoplocephalus* was simply a byproduct of
481 ankylosaurian phylogeny and ecology. *Euoplocephalus* and *Panoplosaurus* represent the two
482 major divisions of the clade Ankylosauria [1, 58]. Currently, our knowledge of nasal passage

483 shape in ankylosaurs is limited to these two taxa. However, if the more extensive “paranasal
484 sinus system” of ankylosaurids [16,18] is an indication of a more convoluted nasal vestibule,
485 then ankylosaurids would have apomorphically elaborated their nasal passages to a greater
486 degree than nodosaurids. The driving force behind the more extensive elaboration of the nasal
487 vestibule in ankylosaurids over nodosaurids is difficult to determine. The notably divergent
488 cranial architecture in these two taxa likely played an important part. Nodosaurid skulls are
489 longer than they are wide, appearing pyriform in dorsal view, whereas ankylosaurid crania are
490 decidedly squatter with broad and blunt rostra [12]. The more restricted cranial real estate in
491 ankylosaurids would necessitate greater convolutions to obtain an equivalent airway length to
492 nodosaurids. With that said, it is pertinent to note that the length of the nasal vestibule in
493 *Euoplocephalus* greatly exceeds that observed in *Panoplosaurus*, regardless of convolutions
494 (Table 6). Based on our mass estimates of these two taxa, *Euoplocephalus* was 1.7–1.8 times
495 larger than *Panoplosaurus*. However, the cavity housing the nasal vestibule of
496 *Euoplocephalus*—as preserved in the cranium—was just over twice the length and nearly 3 times
497 the volume of the preserved nasal vestibule cavity in *Panoplosaurus*. Skull architecture does not
498 appear to fully explain the discrepancy in nasal passage length between these two taxa.
499

500 **Table 6. Nasal vestibule size compared with body mass and endocast volume**

Taxon	Vestibule length (mm)	Vestibule volume (mm³)	Body mass (kg)	Endocast volume* (mm³)
<i>Panoplosaurus</i>	400	157134	1100–2000	699.5
<i>Euoplocephalus</i>	808.74	436740	2000–3500	811.5

501 *Endocast volume obtained from segmentations of endocranial cavity by Witmer & Ridgely
502 [20,21]

503 Cranial differences between nodosaurids and ankylosaurids have been argued to be a
504 response to the different dietary niches of these two ankylosaur clades. The narrower snouts of
505 nodosaurids suggest a more selective feeding strategy, as compared to the bulk feeding proposed
506 for ankylosaurids [74]. The Dinosaur Park Formation has been interpreted as housing both open
507 and closed habitats [74]. If ankylosaurids were less discerning in their diets and relied heavily on
508 hindgut fermentation, they could have spent more time grazing in open terrain. This extensive
509 time under a constantly-beating sun, coupled with the heat produced from vast quantities of
510 fermenting vegetation in the gut, may have placed a higher heat load on the brain of
511 *Euoplocephalus*, as opposed to *Panoplosaurus*, which could have spent more time in covered
512 habitat, with less reliance on hindgut fermentation of low-quality ingesta. Although this scenario
513 is largely speculative, it would align with previous work on dental microwear and expected diets
514 in ankylosaurids as compared to nodosaurids [74,75].

515 A final factor to consider is the overall size difference between these two ankylosaurs.
516 *Euoplocephalus* was 900–1500 kg more massive than *Panoplosaurus* based on estimates from
517 Brown et al. [76]. Larger animals—with their lower surface-area-to-volume ratios—absorb,
518 produce, and retain more heat than smaller animals [77]. As a substantially more massive animal,
519 *Euoplocephalus* would have been capable of absorbing higher heat loads than its lighter relative.
520 Elaboration of the nasal apparatus could have been an evolutionary response to offsetting these
521 larger heat loads. The Dinosaur Park Formation featured two other ankylosaurs during this time
522 period. The nodosaurid, *Edmontonia rugosidens* and the ankylosaurid *Dyoplosaurus*
523 *acutosquameus*. Both taxa are known from enough material to provide fairly accurate estimates
524 of their body mass [76]. Notably, both ankylosaurids had higher estimated body masses for a

525 respective body length than their nodosaurid relatives (Table 7). Ankylosaurids appear to have
526 been heavier nodosaurids for any given body length.

527

528 **Table 7. Size estimates of ankylosaurs from the Dinosaur Park Formation**

Taxon	Estimated length (m)	Estimated mass (kg)*
<i>Dyoplosaurus</i>	3.58–4.16†	1500–2500
<i>Euoplocephalus</i>	5–6†	2000–3500
<i>Edmontonia</i>	6‡	1000–1800
<i>Panoplosaurus</i>	5‡	1100–2000

529 *from [76]. † from [78]. ‡ from [79]

530 The potentially more massive bodies in ankylosaurids suggests that a potential causal
531 relationship between nasal passage complexity and body size may exist. This relationship aligns
532 well with the heat transfer results from our simulation study. Further supporting this causal
533 relationship was a recent CT analysis of the small, basal ankylosaur *Kunbarrasaurus ieverisi*
534 [80]. The authors discovered its nasal passage to be remarkably short and potentially simplistic,
535 which suggests that ankylosaur nasal passages became more elaborate as members of the clade
536 grew larger. However, *Kunbarrasaurus* did also live in a different environment and time from
537 the ankylosaurs in our current study, and thus was likely subjected to a different set of
538 environmental pressures. Detangling nasal passage shape from the multiple factors of ecology,
539 phylogeny, and biology is a topic in of itself that is beyond the scope of this study. It is likely
540 that a mix of all three of these factors drove the evolution of nasal passage elaboration in
541 ankylosaurs. Further, these results do not negate potential alternate functions of the nasal
542 passage, especially in regard to vocal resonance. Our results only indicate that the elaborate nasal
543 passages of ankylosaurs had the potential to be efficient heat exchangers, even if that was not
544 their primary function.

545

546 **Fig 15. Airway reconstruction and soft-tissue correction in *Panoplosaurus mirus* (ROM**
547 **1215).** (A) Initial CT-based bony-bounded segmentation of airway within the skull and (B)
548 isolated BB airway. (C) Airway cleaned and separated, with the addition of a soft-tissue naris
549 and nasopharyngeal duct exiting into an artificially created laryngotracheal region. (D) Nasal
550 passage digitally compressed to reduce airway caliber, better simulating the mucosa-lined
551 airways of extant amniotes. Black lines indicate locations of cross sections (E–F). (E) Cross
552 section of original BB airway caliber. (F) Cross section of airway after soft-tissue correction.

553 **Fig 16. Airway reconstruction and soft-tissue correction in *Euoplocephalus tutus* (AMNH**
554 **5405).** (A) Initial CT-based bony-bounded segmentation of airway within the skull and (B)
555 isolated. (C) Airway cleaned and separated, with the addition of a soft-tissue naris and
556 nasopharyngeal duct exiting into an artificially created laryngotracheal region. (D) Nasal passage
557 digitally compressed to reduce airway caliber, better simulating the mucosa-lined airways of
558 extant amniotes. Black lines indicate locations of cross sections (E–F). (E) Original bony-
559 bounded airway caliber. (F) Airway caliber after soft-tissue correction.

560 **Fig 17. Alternate airway models for *Panoplosaurus mirus*.** (A) Dorsal view of the straightened
561 airway (removal of nasal vestibule curvature) and the original, ST-corrected airway. (B) Lateral
562 view of skull of *P. mirus* (ROM 1215) with basic airway in situ. A direct connection between the
563 bony narial aperture and the CNP in a loss of 55% of the original nasal vestibule.

564 **Fig 18. Alternate airway models for *Euoplocephalus tutus*.** (A) Dorsal view of the
565 straightened airway (removal of nasal vestibule curvature) and the original, ST-corrected airway.
566 (B) Lateral view of skull of *E. tutus* (AMNH 5405) with basic airway in situ. A direct connection

567 between the bony narial aperture and the CNP resulted in a loss of 80% of the original nasal
568 vestibule.

569 **Nasal convolutions vs. respiratory turbinates**

570 Regardless of the relative efficiency between these two ankylosaurs, both animals seemed
571 quite capable of modifying respired air. That both dinosaurs were able to modify respired air
572 without the aid of respiratory turbinates or conchae is particularly intriguing. Respiratory
573 turbinates—and the physiologically active mucosal conchae that reside on them—have been
574 hypothesized to have evolved strictly for the function of increasing the water reclaiming ability
575 of the nasal passage, mitigating the effects of high ventilation rates as seen in mammalian
576 endotherms [34,35,38,39]. However, as has been previously suggested [81,82], this necessity for
577 respiratory turbinates appears to be truer for mammals than for sauropsids, as the latter have
578 markedly lower ventilation rates than equivalently sized mammals [49,81]. The estimated resting
579 breathing frequency of *Panoplosaurus* and *Euoplocephalus* was 1.5 and 1.2 breaths/minute,
580 respectively. Such slow breathing would result in naturally low rates of respiratory evaporative
581 water loss (REWL) regardless of whether respiratory turbinates were present. As such, the need
582 for a water recovery mechanism may not have been as strong a selective force as it appears to be
583 in mammals, allowing for alternate means of solving the REWL problem, such as evolving a
584 long, winding nasal passage. Our results indicate that an elongated, convoluted nasal passage
585 produces equivalent results to a turbinate-filled airway. Both anatomical organizations appear to
586 offer the same results albeit with different tradeoffs. A single, winding airway warms and
587 transports air in a stepwise, serial fashion. In contrast, a turbinate-filled airway breaks the air
588 field into multiple, parallel-running air streams. The latter approach appears to function well at
589 warming large volumes of air in a relatively small space, allowing a short airway to act like a

590 long airway [83]. However, by breaking the airfield into a series of smaller streams, turbinates
591 also decrease the caliber of the airway in these regions. Intuitively, we should expect to see a
592 concomitant, and rather large, increase in airflow resistance as determined from a derivation of
593 the Hagen-Poiseuille equation [71]:

$$594 \quad R = \frac{8\mu l}{\pi r^4} \quad (1)$$

595 where R = resistance, μ = dynamic viscosity, l = the length of the “pipe” and r = the radius of the
596 “pipe.” As indicated by the exponent in the equation, resistance is highly sensitive to the radius
597 of the structure through which a fluid flows. Separating the airfield into a series of smaller air
598 channels should result in a substantial increase in airway resistance. However, even though
599 turbinates break up the airway into multiple channels, these channels are all running in parallel to
600 each other. Unlike resistance in a serial system of pipes, the cumulative resistance in a turbinate-
601 filled airway—much like in an electrical circuit—is best calculated by taking the reciprocals of
602 resistance for each parallel channel [71]:

$$603 \quad R_{total} = \sum \frac{1}{\frac{1}{R_1} + \frac{1}{R_2} + \frac{1}{R_3} \dots} \quad (2)$$

604 Thus, an airway split into multiple parallel channels will increase in resistance much
605 slower than it would appear at the outset, which makes the filling of nasal passages with
606 turbinates an energetically viable option (Fig. 19). Standard scaling rules indicate that an
607 isometric increase in body size will increase the volume of the nasal passage [77]. Van
608 Valkenburgh et al. [84] found the turbinate-filled nasal passages of carnivorans to scale
609 positively allometrically, thus indicating even larger increases in airway volume with body size
610 than predicted from isometry. Increasing nasal passage volume should reduce the efficacy of the
611 nasal passage at transferring heat, due to the diffusion limited nature of heat transfer discussed
612 earlier. However, increasing the volume of a turbinate-filled nasal passage results in a relatively

613 minor increase in the gap distance between opposing turbinate walls. Thus, an increase in nasal
614 cavity volume should result in only modest increases in individual channel volume. The larger
615 size of the nasal cavity may further be compensated for by changing the arrangement of
616 individual turbinates (e.g., increased scrolling) or increasing the thickness of the mucosa that
617 resides on them (conchae). This ability to slow the rate of radial distance increase within the air
618 field appears to make nasal turbinates more resistant to changes in body size than a serially-
619 arranged nasal passage may be. This resilience may explain why turbinate density appears to not
620 scale with body size in carnivoran mammals [84]. In contrast, a single long airway offers lower
621 resistance, but it does impose a limit on how much air can be processed at any one time.
622 Increasing heat-transfer efficiency—or maintaining it at larger sizes—requires more contortions
623 of the nasal passage, filling up more space within the skull and increasing anatomical dead space
624 within the conducting portion of the respiratory system. For slow-breathing animals this
625 limitation on airflow processing is less of a problem. Among extant diapsids, the nasal passages
626 of ankylosaurs are reminiscent of the winding airways found in some lizards [85], such as
627 *Uromastyx* (Fig. 20). Lizards—much like birds—are slow breathers compared to similar sized
628 mammals [86], and the limitation on air processing imposed by a long, serial airway does not
629 seem to affect them. Further the likely presence of a unidirectional airflow system in the lungs of
630 dinosaurs [87,88], and possibly all diapsids [89–91], would further offset any increases in
631 anatomical dead space.

632

633 **Fig 19. Example of flow in a hypothetical, serial pipe (top) vs. a parallel pipe (bottom).**

634 Resistance is sensitive to the pipe's caliber, giving the parallel pipe greater resistance on the
635 outset. However, the parallel arrangement of the smaller caliber tubes offsets some of the

636 increased resistance, resulting in only a modest increase in overall resistance, while
637 simultaneously increasing surface area to volume ratios. In the above example, the parallel pipe
638 has half the caliber of the serial pipe, but is split into fourteen partitions, resulting in
639 approximately identical resistance to the single, serial pipe.

640 **Fig 20. Airway of the lizard *Uromastix aegyptia* (OUVC 10688) in (A) oblique left lateral**
641 **and (B) dorsal view.** As with ankylosaurs, the nasal passage (yellow) exhibits convolutions that
642 increase surface area. (C) Horizontal CT slice image reveals that “slabs” of mucosa are
643 responsible for compressing the airway. It is likely that these mucosal slabs are well
644 vascularized, which would aid in heat and water savings during respiration in this taxon.

645 **Nasal air conditioning and brain cooling**

646 Although much has been written on the heat and water retaining function of respiratory
647 turbinates [34–39] as well as the nasal passage itself [28,29,31–33], fewer studies have looked at
648 the other side of this nasal function, namely, its ability to dump excess heat from the body core.
649 Inspired air is heated in the nasal passage by pulling heat away from warm blood coursing
650 beneath the adjacent mucosa. As such, the nasal passage not only warms and humidifies inspired
651 air, but it also acts as a heat sink for hot blood coming from the body core. Blood vessels that
652 surround the nasal passage have the potential to shed excess heat, resulting in a source of cooled
653 blood. An extensive survey of vasculature in extant sauropsids [72,92–94] found that the nasal
654 passage is supplied by predictable branches from the internal and external carotid arteries. These
655 arterial branches supply capillary beds within the nasal mucosa that transition into major venous
656 pathways that course caudally towards the brain and eyes. Reconstructed vasculature in
657 dinosaurs, including the ankylosaurs used in this study ([20], Fig. 14), has revealed extensive

658 nasal vasculature in large-bodied dinosaurs with pathways similar to those of extant diapsids
659 [72,81,92]. Shedding excess body heat in the nasal passages provides a means for sauropsids to
660 keep their brains from overheating and maintain an independent and physiologically optimal
661 temperature range. Studies on extant amniotes have found that head temperature tends to be
662 more strictly regulated than body temperature [95–99]. The oronasal apparatus has long been
663 implicated in controlling these body temperature differences [99–103]. Many studies have
664 focused solely on the role of the oronasal apparatus in avoiding heat stress (e.g., [103]). These
665 studies tended to observe other signs of heat stress (e.g., panting) that have been shown to offer a
666 means of locally cooling the cephalic region of the body [101–103]. Our ankylosaur data,
667 however, indicate that a substantial blood cooling capacity in the nasal passage was present even
668 under “relaxed” or resting conditions (i.e., not heat stress). We speculate that heat dumping in
669 these enhanced nasal passages may have been more obligate as the large size of these dinosaurs
670 would have resulted in a very high heat load that—when transferred to remarkably small brains
671 ([83], Table 6)—would have created conditions that would continuously place the brain at risk of
672 overheating. Interestingly, similar nasal elaborations have been observed in sauropods,
673 ornithopods, and ceratopsians [105]. All of these groups are comprised of mostly large bodied
674 (multi-tonne) animals. As with ankylosaurs, these dinosaur taxa also reveal elaboration of the
675 nasal vestibule. The nasal vestibule appears to be the most plastic of nasal passage anatomy, as it
676 is also the most variable part of the nose in birds, turtles, and lizards [106–109]. [] Nasal
677 vestibule elaboration in sauropods, hadrosaurs, and ceratopsians may have evolved for brain
678 cooling in these taxa as well. Future work looking at more basal members of these dinosaur
679 groups (e.g., the basal ankylosaurian, *Kunbarrasaurus* [110]) will provide greater insight into the
680 role of nasal passage elaboration and body size evolution in dinosaurs.

681 **Materials and Methods**

682 **Specimens**

683 We analyzed airflow in two species of ankylosaur, the nodosaurid *Panoplosaurus mirus*
684 (ROM 1215) and the ankylosaurid *Euoplocephalus tutus* (AMNH 5405). CT data and initial 3D
685 models were obtained from previous work conducted by Witmer & Ridgely [20]. To aid with
686 soft-tissue reconstruction, we further looked at other specimens of *Euoplocephalus* (AMNH
687 5403, ROM 1930) and *Panoplosaurus* (CMN 2759) as well as the related species: *Edmontonia*
688 *rugosidens* (AMNH 5381), *Ankylosaurus magniventris* (AMNH 5214), *Pinacosaurus grangeri*
689 (ZPAL MgD-II/1), and *Kunbarrasaurus ieverisi* (QM F18101).

690 **Model construction**

691 **Segmentation**

692 Osteological evidence for a complete nasal septum (septal sulcus or partially mineralized
693 septum) meant that left and right nasal passages acted independently of each other. This allowed
694 for modeling of one side of the nose only, which saved on computational costs. Initial
695 segmentation of the airways produced a rough approximation of the nasal passage in life,
696 complete with a rostral and caudal vestibular loop [20] and an enlarged olfactory recess (Fig. 2).
697 We refer to the enlarged, looping area of the nasal passages in both ankylosaurs as the nasal
698 vestibule. This demarcation of nasal passage anatomy in sauropsids is typically determined by
699 the placement of the duct for the nasal gland [106,107]. Unfortunately, the duct and its ostium
700 are both soft-tissue structures that do not leave impressions on the bone. As an alternative, we
701 used the region of the nasal passage where nasal cavity diameter suddenly increased [81]. This
702 area is known to correlate with the terminus of the nasal vestibule in extant sauropsids.[111]

703 Further, support for this interpretation comes from the tube-shaped structure of the nasal
704 vestibule in extant reptiles. The morphology of the looping portions of the ankylosaur airways
705 best fits this description. The nasal vestibule and the CNP were unattached to each other in the
706 original airway segmentations [20], requiring further segmentation and attachment to produce a
707 contiguous surface model. The nasopharyngeal duct was not segmented in the original models
708 and required segmentation. Although Witmer and Ridgely [20], as well as Miyashita et al. [21],
709 discussed the presence of well-preserved olfactory turbinates within the olfactory recess of these
710 dinosaurs, neither study published images of the segmented structures. For our study, these
711 structures and their effect on the airway (i.e., the impressions they left on the digital airway cast)
712 were segmented using the program Avizo 7.1 (FEI Visualization Sciences Group, Burlington,
713 MA). As with the initial airway segmentation, the final product was a cast of the inside of the
714 nasal cavity, revealing the potential space in which air could reside within the nasal passage.
715 Examination of the CT data within the olfactory recess revealed both the presence of mineralized
716 olfactory turbinates as well as the outer boundary to the nasal capsule. These data provided
717 insight into the limit of the airway in life, which was substantially more restricted than initial
718 segmentations suggested (Fig. 21). Extra space lateral to our interpretations of the nasal passage
719 wall was interpreted as housing the antorbital sinus. Its placement near the olfactory chamber,
720 adjacent to the CNP, is consistent with antorbital sinus placement in extant archosaurs [14]. In
721 preparation for meshing, the segmented models were cleaned of segmentation artifacts using the
722 program Geomagic 10 (3D Systems Geomagic, Rock Hill, SC).

723

724 **Fig 21. Segmentation of the airway in *Panoplosaurus mirus* (ROM 1215). (A) Skull in left**
725 **lateral view. Line represents the location of (B) axial CT section showing preserved olfactory**

726 turbinates. (C) Diagram of CT image showing caliber of airway vs. entire nasal cavity. (D)
727 Segmented olfactory turbinate in same plane as CT image.

728

729 **Fleshy nostril placement and soft palate**

730 Although ROM 1215 and AMNH 5405 both contained well preserved nasal passages, the
731 terminal regions of the nose—the fleshy nostril and choana—were not preserved. To aid with
732 these soft-tissue reconstructions we turned to other specimens of the same species along with
733 well-preserved specimens of related ankylosaurs to better determine the location of the nostril
734 and choana.

735 **Fleshy nostril**

736 For *Panoplosaurus*, we used the well-preserved skull of CMN 2759 to determine the
737 location of the nostril. CMN 2759 preserved the rostral wall of the bony narial aperture, which
738 was comprised of the rostral-most cranial osteoderm, most similar to the median nasal
739 caputegulum of *Euoplocephalus* [112]. These anatomical structures strongly suggested that the
740 nostril of *Panoplosaurus* deviated laterally (Fig. 22A,C). Laterally-facing nostrils are common
741 among diapsids and such a placement in *Panoplosaurus* was not unexpected.

742

743 **Fig 22. Nostril placement in ankylosaur models. All skulls in right lateral and rostral views.**

744 For *Panoplosaurus mirus* (A, C) we used (A) ROM 1215 as our base model with nostril
745 placement informed by (C) CMN 8530. For *Euoplocephalus tutus* (B, D) we used (B) AMNH
746 5405 as our base model with the skull of (D) ROM 1930 informing us on the limits to the extent
747 of the nostril. Asterisks in A and B denote location of fleshy nostril in our models.

748 For *Euoplocephalus*, AMNH 5405 did not present a well-preserved rostral-most portion
749 of the cranium. To assist with nostril positioning, we compared bony narial aperture shape in
750 AMNH 5405 with ROM 1930 (Fig. 22B,D). In the latter, preservation of the rostral-most region
751 of the cranium revealed an enlarged bony narial aperture that faced forward suggesting terminal
752 nostril placement. However, the width of the bony narial aperture encompassed both the rostral-
753 most portion of the cranium as well as a lateral portion of the cranium. Thus, it remains possible
754 that the nostril in *Euoplocephalus* could have deviated laterally, or had a rostromedial
755 combination thereof. This position would be consistent with fleshy nostril placement in
756 *Ankylosaurus* (AMNH 5214) where dermal ossification is extensive and indicates
757 unambiguously that the nostril was located rostroventrolaterally [78]. In contrast,
758 *Anodontosaurus lambei* (CMN 8530), a close relative of *Euoplocephalus*, shows a well
759 constrained bony narial aperture that would limit the nostril to a terminal position on the snout
760 [112]. All known skulls of *Euoplocephalus* that preserve the rostral-tip of the snout show a much
761 less constrained bony narial aperture. This could indicate that the caputegula covering the
762 cranium were less extensive in this species and that terminal fleshy nostrils were present but
763 were constrained only by soft-tissues. AMNH 5405 has a fossa on the premaxillae (apertura
764 nasalis [17]) that has previously been interpreted as a portion of the nasal vestibule ([17,20], Fig.
765 21B,D). This fossa is wide enough that it could have easily housed a laterally deviating nasal
766 vestibule that terminated rostrally in a laterally-facing nostril. For the purposes of our analysis
767 we fit *Euoplocephalus* with such a nostril, with the caveat that the osteological evidence for it
768 was equivocal (Fig. 22B,D). Such a position is consistent with the general finding in amniotes
769 that fleshy nostrils tend to be rostroventrally situated within the nasal vestibule [113].

770 **Choana**

771 The choana is the fleshy, “internal nostril” for the nasal passage. It represents the
772 terminus of the airway within the nasal passage as the airway passes into the throat. Much as
773 how the fleshy nostril resides within the larger narial fossa, the choana is typically associated
774 with a much larger structure called the fenestra exochoanalis [88,89, Fig. 23] or bony choana
775 [81]. The difference in shape between the fleshy and bony structures varies across species. In
776 birds, the fenestra exochoanalis is extensive. It is bordered by the palatines laterally and
777 caudally, the vomers medially, and the maxilla rostrally [115]. The choana opens as a fleshy slit
778 at the caudal terminus of the fenestra exochoanalis in birds, and is often covered in life by
779 “choanal flaps” that keep food particles out of the nasal passage during ingestion [116,117].
780 Osteologically, the choana is associated with a depression in the palatines referred to as the
781 choanal fossa ([116], Fig. 23B). Lizards have a choanal morphology similar to birds (Fig. 23C).
782 Their extensive fenestra exochoanalis is bounded by the maxillae rostrally and laterally, the
783 palatines caudally and medially, and the vomers medially. As with birds, the choana resides at
784 the caudal-most extent of the fenestra exochoanalis [118,119]. However, unlike birds the fleshy
785 covering of much of the fenestra exochoanalis is less extensive and food appears to be prevented
786 from entering the nasal passage partially by the more lateral placement of the choana on the oral
787 roof along with a well-developed choanal fold that extends the majority of the length of the
788 fenestra exochoanalis ([119], Fig. 23C). As with birds, lizard choanae are associated with a
789 choanal fossa (= choanal groove, [118,119]) situated at the caudal-most extent of the fenestra
790 exochoanalis. Depending on the lizard species, the choana either opens or is greatly expanded in
791 this region of the fenestra exochoanalis (Fig. 23C). Crocodylians have an apomorphic choana
792 placement referred to as the secondary choana [109]. It is produced via elongation of the
793 nasopharyngeal duct through the palatines and into the pterygoids. The original or primary

794 choana is still present and can be viewed internally within the dried skulls of extant crocodylians,
795 where Witmer [109] observed it bounded medially by the vomer, caudally by the palatines and
796 vomer, and laterally by the palatines and maxillae. These bony associations agree with choana
797 placement in birds and lizards, thus suggesting that the primary choana is the location of the
798 fenestra exochoanalis. The soft-tissue of the secondary choana is essentially an identical outline
799 of the underlying bone, negating the need for a separate term for this region. Thus, the exit of the
800 nasal cavity in crocodylians, regardless of soft-tissue presence, is the secondary choana (Fig.
801 23A). Using the extant phylogenetic bracket approach (EPB, [120]), the presence of a choanal
802 groove/fossa in both birds and lizards, can be considered a shared trait for diapsids that was later
803 lost in crocodylians, making the choanal groove/fossa a level 1 inference for placement of the
804 choana in the fenestra exochoanalis of diapsids [81].

805

806 **Fig 23. Lateral and ventral views of extant diapsid skulls illustrating the location of the**
807 **choana.** Crocodylians such as (A) *Alligator mississippiensis* (OUVC 9412) have a greatly
808 retracted, apomorphic secondary choana. *Inset:* The bony boundaries to the secondary choana
809 correspond to the soft-tissue boundaries. Birds such as (B) *Meleagris gallopavo* (OUVC 9647)
810 retain the plesiomorphic placement of the choana. *Inset:* Magnified palatal region showing the
811 difference between the bony boundaries to the choana (left side of image) and the soft-tissue
812 boundaries (right side of image). Lizards such as (C) *Iguana iguana* (OUVC 10446) similarly
813 show the plesiomorphic position of the choana. *Inset:* Relationship between the bony boundaries
814 to the choana (left side of image) and the more restricted soft-tissue boundaries (right side of
815 image).

816 Both *Panoplosaurus* and *Euoplocephalus* had extensive fenestrae exochoanales (Figs.
817 24–25). The shape of the soft palate in ankylosaurs has not been extensively studied. However,
818 details on the hard-tissue anatomy indicate that despite an enlarged fenestra exochoanalis, there
819 is evidence of bony secondary palate formation [1,13,17,121]. The secondary palate of
820 ankylosaurs has traditionally been viewed as a bipartite structure [13]. Rostrally, elongated
821 vomers contact the premaxilla, which sends out medial processes along with the maxilla to form
822 palatal shelves, making a structure referred to as the “rostradorsal secondary palate” [13,121].
823 Caudally, the palatines join with the vomers and pterygoids to form a structure called the
824 “caudodorsal secondary palate” [13,17,121]. In light of new information on the shape of the
825 nasal passage in ankylosaurs, the terminology for the palatal region of ankylosaurs should be
826 revised. The rostradorsal secondary palate in ankylosaurs such as *Euoplocephalus* should be
827 viewed as the secondary palate (Fig. 24), which is consistent with the usage of the term in other
828 tetrapods in which the premaxillae and maxillae (and sometimes even palatines) meet rostral to
829 the choanae [122]. The “caudodorsal secondary palate” serves to separate the olfactory recess
830 from the rest of the nasal cavity. This structure is equivalent to the nasal structure known in
831 mammals as the lamina transversa ([48,123,124], Fig. 24C) and thus takes no part in the
832 formation of the definitive palate. Crocodylians exhibit a similar partitioning of the nasal
833 passages, with the roof of their nasopharyngeal duct forming the floor of their olfactory recess
834 [109]. A large depression in the caudal aspect of the palatines appears equivalent to the choanal
835 fossa or choanal groove seen in most extant diapsids (Figs. 23–24). As such, we interpret this
836 region as the opening of the choana into the throat. This interpretation makes the lamina
837 transversa the bony boundary for an elongate nasopharyngeal duct. In nodosaurids such as
838 *Panoplosaurus*, the distinction between the secondary palate and the choana is more evident

839 [19,125], Fig. 25). As with *Euoplocephalus*, there is evidence of a choanal fossa on the caudal
840 aspect of the palatines, suggesting that the choana opened caudally in this taxon as well (Fig. 25).

841

842 **Fig 24. Palate identification and placement in *Euoplocephalus tutus* (AMNH 5405).** (A)

843 Skull in lateral and (B) ventral view. *Inset*: Major features of the palatal region. We refer to the
844 caudodorsal secondary palate as equivalent to the lamina transversa observed in many mammals
845 (C). Image in C modified from Cave [124].

846 **Fig 25. Palate identification and choana placement in *Panoplosaurus mirus* (ROM 1215).**

847 (A) Skull in lateral and (B) ventral view. *Inset*: Major features of the palatal region.

848 **Soft-tissue correction**

849 Airways segmented from the skulls represented the outer limits of the nasal passage,
850 referred to here as the bony-bounded (BB) airway (Figs 15C–16C). In life, soft tissues within the
851 nasal passage such as the nasal capsule cartilages, mucosa, nerves, and vasculature would have
852 been present and would have occupied space within these well-constrained nasal passages (Fig.
853 26). Previous surveys of airway calibers in the nasal passages of extant amniotes found that
854 airway caliber (the distance spanned between mucosal walls) does not exceed 10 mm in diameter
855 regardless of the size (0.1–600kg) or phylogenetic position (from squamate reptiles to artiodactyl
856 mammals) of the animal [33,81]. This constraint appears to be dictated by the biophysical
857 limitations of diffusion, which effectively works across only very small distances [71]. The
858 thermoregulatory and olfactory functions of the nasal cavity are both diffusion-dependent
859 functions [29,31,126]. In contrast to data from extant animals, the average BB airway calibers in
860 *Panoplosaurus* and *Euoplocephalus* were 15.8 mm and 22.9 mm, respectively. These were

861 significantly larger calibers than that observed in the mucosa-lined airways of extant amniotes.
862 To bring airway calibers within the range observed in extant amniotes, we imported airway
863 models of *Panoplosaurus* and *Euoplocephalus* into the 3D modeling and animation program
864 Maya (Autodesk, San Rafael, CA) where the airways were compressed using the program's 3D
865 deformation tools. Airway calibers were reduced until the average diameter was ~10 mm, which
866 is the upper limit observed in extant amniotes, making this a conservative estimate for
867 ankylosaurs. Airway compression followed the natural contours of the nasal passage such that
868 the refined airways resembled a more compressed version of the original segmentation (Figs. 15–
869 16). These soft-tissue-corrected airways are here referred to as the ST airways (Figs. 15D–16D).
870 An extension off the choana was added to all models tested. This extension served to replicate
871 the connection of the nasal airway to the larynx and trachea. This extension was added to address
872 technical aspects of the software (see below) and to ensure that fully developed airflow would be
873 present at the choana during expiration, thus removing any potential heat flow artifacts created
874 by having the program initialize airflow at the choana during expiration (Figs. 15–16).

875

876 **Fig 26. Generic airway diagram for diapsids.** Note the much more constricted airway in the
877 soft-tissue nasal passage (A) vs. the emptier, bony-bounded nasal passage typically preserved in
878 fossils (B).

879 To further test the hypothesis that the convoluted airways in our two ankylosaur taxa
880 were conferring a heat-transfer benefit, we digitally manipulated duplicates of our ST airways to
881 remove either the length or the convolutions from the nasal vestibule (Figs. 17–18). One version
882 had a nasal vestibule that extended the straight-line distance between the nostril and the CNP.
883 This model, referred to as the basic airway (Figs. 17B–18B), was used to represent what a

884 simplified or plesiomorphic nasal vestibule would look like. The second version of the ST
885 airway retained the total length of the nasal vestibule but had the curvature of the airway
886 removed (Figs. 17A–18A). This model was referred to as the straightened airway. It represented
887 the effects of airway distance alone on heat transfer through the nasal passage.

888 **Boundary conditions**

889 Prior to volumetric meshing, the airway models were assigned a series of boundary
890 conditions comprising a set of criteria that described this region of the model to the CFD
891 program. Boundary condition assignment was done to elicit physiologically realistic airflow
892 within the nasal passage (i.e., pressure driven air movement between nostril and choana). These
893 conditions consisted of a pressure inlet located at the fleshy nostril and a pressure outlet located
894 at the end of the artificial trachea (Fig. 27A). During expiration, the assignment of these
895 boundary conditions (inlet and outlet) was swapped. A series of impermeable wall boundaries
896 covered the rest of the nasal passage model. Wall boundaries were demarcated based on
897 anatomical location (Fig. 27A). This was done to better control for regional variation in heat
898 transfer across the nasal passage. Each wall boundary was considered rigid and incorporated a
899 “no-slip” condition that states that air at the fluid-solid interface would be static, an assumption
900 based on known properties of fluid movement through enclosed structures [71]. Note that
901 amniote nasal passages do not have a truly rigid boundary layer between the mucosa and the air
902 field. Boundary layers act as obstacles to diffusion-based processes, thus it is beneficial for
903 amniotes to have means of reducing the size of these boundary layers. In extant amniotes, there
904 is a mucociliary “conveyor belt” comprised of ciliated epithelium that beats in unison towards
905 the nostril or choana [127,128]. This conveyor belt serves to move mucous across the mucosa of
906 the nasal passage. This movement has the potential to reduce the boundary layer between the

907 mucosa and the air field, which would aid in diffusion of heat and odorant molecules across the
908 air-mucosa boundary. However, the speed of cilia movement is extremely slow (≤ 1 cm/min,
909 [45]) compared to airflow, and its effects on airflow and heat transfer can be considered
910 negligible for the purposes of our study. Thus, our use of a no-slip boundary condition should not
911 hamper or otherwise reduce the quality of our results.

912

913 **Fig 27. Mesh example for *Panoplosaurus mirus* (ROM 1215).** (A) Nasal passage was assigned
914 a series of boundary conditions (color-coded). Black line indicates location of (B) axial cross
915 section illustrating the distribution of volumetric cells within the nasal passage.

916 **Meshing**

917 Volumetric meshing was performed using the meshing program ICEM CFD (ANSYS
918 Inc., Canonsburg, PA). Models consisted of a tetrahedral-hexahedral (tet-hex) hybrid mesh. First,
919 an unstructured tetrahedral mesh was constructed using the robust OCTREE method [129]. After
920 mesh reconstruction, the core of the mesh was deleted and flooded with hexahedra wherever
921 possible. This hybrid construction offered the versatility of tetrahedra for unstructured mesh
922 reconstruction [130,131], coupled with the computational efficiency of hexahedra [132,133]. To
923 better resolve wall boundary effects on heat transfer, we incorporated a prism layer along the
924 wall of the nasal passage. This layer consisted of four cells that grew in size from the wall by 1.5
925 times their parent cell, producing a combined thickness of approximately 0.7 mm (Fig. 27B).

926 **Computational Fluid Dynamic Analysis**

927 Meshes were imported into the CFD program Fluent (ANSYS Inc., Canonsburg, PA) for
928 analysis. To determine the appropriate fluid dynamic model to apply to our airway models, we

929 first took cross sections throughout the nasal passages to determine the dimensionless Reynolds
930 and Womersley numbers for the airway. The Reynolds number is a staple of fluid dynamic
931 analyses [71,134], representing the mathematical relationship between the viscous and inertial
932 forces within a fluid. Low Reynolds numbers (< 2000) indicate that viscous forces dominate the
933 system and that orderly (i.e, laminar) flow will be the dominant flow type expected. Reynolds
934 numbers between 2000–4000 indicate a transition zone in which laminar flow may be punctuated
935 with periods of turbulence that manifest in the form of secondary flows such as Von Kármán
936 trails [71]. Reynolds numbers above 4000 indicate that inertial forces dominate the system and
937 that flow will be chaotic or turbulent [71,134]. We used the following equation to calculate the
938 Reynolds number for the airway [135]:

$$939 \quad Re = \frac{4Q}{Pv} \quad (3)$$

940 where Q = volumetric flow rate (m^3/sec), P = the wetted perimeter in meters [136], and v = the
941 kinematic viscosity of air at 15°C ($1.412\text{e}^{-5} \text{ m}^2/\text{sec}$).

942 We used the dimensionless Womersley number [137] to determine the steadiness of the
943 flow field, or how often airflow was able to produce a steady, parabolic flow profile. This profile
944 is related to the size of the airway, viscosity of the fluid, and frequency of the oscillation (i.e.,
945 breathing rate). Womersley numbers < 1 indicate a quasi-steady flow field that can be modeled
946 as time independent, or steady-state. As the Womersley number climbs above unity, steadiness
947 decreases. At Womersley numbers > 10 the oscillation of the flow is too high for flow to
948 completely develop [138] and is considered unsteady, thus requiring a transient or time-step-
949 based modeling approach. We calculated the Womersley number using the following equation
950 [45]:

$$951 \quad Wo = \frac{Dh}{2} \sqrt{\frac{2\pi f}{v}} \quad (4)$$

952 where f = the frequency of oscillation (Hz), and D_h = hydraulic diameter of the airway.

953 Hydraulic diameter was calculated using the following equation [136]:

954
$$h = \frac{4A}{P} \quad (5)$$

955 where A = the area of the cross section measured (m^2).

956 **Physiological Variables**

957 Following our previous methodology [81], we used the same phylogenetically corrected
958 allometric equation for resting respiration in birds [49] to estimate flow rates during inspiration
959 and expiration (Table 8). Mass estimates for both ankylosaurs were taken from the
960 supplementary data in Brown et al. [73]. Estimated masses for the two ankylosaurs were over 20
961 times larger than the largest animal in the Frappell et al. dataset ([49], an 88 kg ostrich). Using
962 the equations from Frappell et al. [49] required extending the regression line well beyond the
963 initial scope of the data. To alleviate the effects of this approach we used the lightest mass
964 estimates for *Panoplosaurus* and *Euoplocephalus* as provided by Brown et al. ([73], Table 8).

965

966 **Table 8. Respiratory values for the ankylosaurs *Panoplosaurus mirus* and *Euoplocephalus***
967 ***tutus***

Taxon	Mass (kg)*	Tidal volume (ml)†	Breathing frequency‡		Low flow rate‡
<i>Panoplosaurus</i>	1100	34,000	1.5 breaths/min	77 L/min	37 L/min
<i>Euoplocephalus</i>	2000	64,000	1.2 breaths/min)	110 L/min	48 L/min

968

969 We performed a cross-sectional analysis of the airways following the methodology of
970 Bourke et al. [81]. Respiratory flow variables input into the Reynolds and Womersley equations
971 above indicated that both taxa would have had steady flow, but air would have been largely
972 transitional if not completely turbulent within the nasal passages during simulated respiration.

973 The latter result was at odds with previously published results on resting respiration in amniotes.
974 In extant amniotes measured during restful breathing, laminar flow dominates the air field
975 [48,139–141]. Laminar flow is less energetically expensive (due to lower resistance) than
976 turbulent flow and can be expected in animals that are not undergoing strenuous exercise. Our
977 two ankylosaurs did not show this pattern, suggesting that the regression equations we used may
978 not be viable at such large body masses or that ankylosaur body plans were not appropriate for
979 the avian-based equation of Frappell et al. [49]. To reduce the effects of poor flow rate choice,
980 we recalculated airflow rates by rearranging the Reynolds equation to solve for flow rate:

981
$$Q = \frac{(Re)Pv}{4} \quad (6)$$

982 We refer to this new method as the Reversed-Reynolds approach. This approach provides an
983 upper limit to volumetric flow through the nasal passage under relaxed conditions. We set the
984 Reynolds number at 2000 (corresponding to the transition into turbulence) as our constant and
985 recalculated flow rate across the nasal passages. The lowest flow rate obtained from cross-
986 sectional analysis using this Reversed-Reynolds equation was chosen as the new flow rate (Table
987 8). This approach, the first of its kind as far as we know, ensures that laminar flow dominates the
988 air field under simulated respiration.

989 Flow rate has been shown to be the primary variable affecting the efficiency of the nasal
990 passage at managing heat flow [29,70]. With this in mind, we chose to run the ST and BB
991 models under both flow rate estimates. The initial flow rate, estimated from the regression by
992 Frappell et al. [49], was deemed the “high flow rate” condition. Our revised flow rate estimate,
993 calculated using our Reverse-Reynolds method, was deemed the “low flow rate” condition. For
994 the high flow rate condition, we used the Wilcox two-equation κ - ω turbulence model [142] with

995 low Reynolds corrections and shear stress transport. For the low flow rate condition, we used the
996 standard laminar viscosity model for continuity, momentum, and energy.

997
$$\nabla \cdot \vec{u} = 0 \quad (7)$$

998
$$\rho(\vec{u} \cdot \nabla) \vec{u} = \nabla \rho + \mu \nabla^2 \vec{u} \quad (8)$$

999
$$(\vec{u} \cdot \nabla) T = \frac{k}{\rho c_p} \nabla^2 T \quad (9)$$

1000 Where $\vec{u} = \vec{u}(x, y, z)$ = the velocity vector, ρ = the density of air at a given temperature, $T =$
1001 $T(x, y, z)$ temperature at a given time, C_p = the specific heat, and k = the thermal conductivity for
1002 air at a given temperature.

1003 **Environmental conditions**

1004 We simulated sea-level air at 15°C and 50% relative humidity (r.h.), which was within
1005 the range of expected conditions that these dinosaurs would have experienced in their
1006 environment [143,144]. We gave the nasal passages an estimated body temperature of 35°C. This
1007 body temperature fell within the range of core body temperatures typically observed in extant
1008 large terrestrial mammals, birds, and reptiles (Table 5). Density (1102 kg/m³), thermal
1009 conductivity (0.34 W/mK), and specific heat for the mucosal walls (3150 J/kgK) were obtained
1010 from the database provided by the Foundation for Research on Information Technologies in
1011 Society (IT'IS). Nasal walls were given a thickness of approximately 0.5 mm for heat to conduct
1012 through. This distance simulated the distance between the nasal passage and the adjacent blood
1013 vessels and was based on observed CT data from extant amniotes [145]. Humidity was simulated
1014 by using the species transport option in Fluent, which allows for the incorporation of the mass
1015 fractions of water at various temperatures (i.e., relative humidity). The nasal walls were assumed

1016 to be at 100% relative humidity during both phases of respiration, following observation on
1017 extant animals [146].

1018 Pressure and velocity coupling used the SIMPLEC algorithm along with a node-based
1019 discretization gradient. We used a second order accurate spatial discretization scheme for
1020 pressure, momentum, turbulence (when applicable), and energy.

1021 Models ran until the results obtained from each analysis had reached a specified level of
1022 stability and consistency referred to as convergence [147]. This indicated that the numerical
1023 process used to solve the problem had asymptotically approached the “true” solution (i.e.,
1024 airflow and heat transfer through a real nasal passage) given the conditions provided to the
1025 program. In CFD, convergence may be determined based on the global imbalances in the values
1026 for each node within the mesh between steps, or iterations, of the model. Imbalances, or errors,
1027 between each iteration are referred to as residuals [147]. The smaller these residuals are, the
1028 smaller the error is and the more converged the solution becomes. Global variables for
1029 momentum, pressure, and continuity (the conservation of fluid mass) are generally considered
1030 solved when their residuals have fallen below $1.0e^{-3}$ [147]. However, for physiological studies
1031 such as ours, we applied the stricter criterion of $1.0e^{-4}$ [45,81]. For energy (heat flow),
1032 convergence is determined when the residuals of error had fallen below $1.0e^{-6}$. To further aid in
1033 determining convergence we monitored special surfaces placed throughout regions of the model.
1034 These surfaces were designed to output data from a single location only (point surfaces). They
1035 provided localized measures of convergence and were used in conjunction with standard
1036 convergence measures for continuity, momentum, and energy to determine when models had
1037 been sufficiently solved.

1038 **Mesh Independence**

1039 To ensure that the results obtained from our analyses were independent of the mesh
1040 resolution, we performed a solution-based adaptive mesh refinement (AMR), following
1041 previously established protocols [83]. This approach used converged or a mostly converged
1042 solution to determine regions of the mesh that had poor resolution. Local refinement was
1043 performed in these regions of poor resolution and the analysis was run again. This approach was
1044 repeated until refined meshes return values that fell below a pre-determined threshold. For our
1045 analysis, we used a threshold of 1% for regional temperature values as determined from point
1046 surfaces (Fig. 28).

1047

1048 **Fig 28. Final model resolutions used for simulations.** Surrounding graphs show sample
1049 adaptive mesh comparisons between different model resolutions for temperature and velocity
1050 within parts of the nasal vestibule.

1051

1052 **Post processing and heat flow measurements**

1053 Solved models were exported to the CFD module of Avizo (Avizo Wind) where
1054 qualitative and quantitative measurements were taken. For heat flow, we took measurements
1055 from cross sections of the nasal passage. These cross sections were taken orthogonal to the
1056 curvature of the nasal passage. Multiple measurements were taken from each cross section and
1057 the mean was recorded for each cross section.

1058 **Caloric costs and savings**

1059 Calculating the energetic costs of heating a single bolus of air by 20°C requires
1060 knowledge of the mass of air being moved between breaths, coupled with the caloric cost of

1061 heating that bolus of air. We calculated our estimated energetic costs using the following
1062 equation:

$$1063 \quad \text{heating cost (cal)} = (M_{air} * Cp) * \Delta T \quad (10)$$

1064 where M_{air} = the mass of air in a given tidal volume (g), and Cp = the specific heat capacity of
1065 air, which is 0.24 cal/g°C across most physiological temperatures [146]. ΔT is the temperature
1066 change the air volume goes through (°C).

1067 The mass of air present in a single breath was determined by multiplying the tidal volume
1068 of air respired, by its density at 35°C, as shown in the following equation:

$$1069 \quad M_{air} = V_T * 1.146 \quad (11)$$

1070 where V_T = the tidal volume (L) and 1.146 = the density of air (g/L) at the estimated body
1071 temperature of 35°C. Body-temperature air density will be the limiting factor behind tidal
1072 volume within the lungs. To determine tidal volume, we used the equation relating tidal volume
1073 to body mass (M) in birds [49].

$$1074 \quad V_T = 20.3M^{1.06} \quad (12)$$

1075 Much of the heat loss from the nasal passage occurs via evaporation of water off the nasal
1076 mucosa [146]. Thus, along with the caloric cost of temperature change within the nasal passage
1077 (sensible heat), one must also take into account the caloric cost associated with the phase change
1078 of water from a liquid to a gas (latent heat). We used saturated steam table values to determine
1079 the latent heat of vaporization for our temperature range. The caloric cost of heating air by 20°C
1080 was calculated using the following equation:

$$1081 \quad \text{heating cost}_{(latent)} = \Delta M_{H_2O} \cdot \Delta H_{vap} \quad (13)$$

1082 where ΔM_{H_2O} = the absolute difference in the mass of water (kg) at two given humidities. ΔH_{vap}
1083 = the latent heat of vaporization for a given temperature (cal/kg). The mass of water was

1084 determined by multiplying the mass fraction of water at a given humidity (g/kg), by the mass of
1085 air (kg) in a single tidal volume.

1086 As heat is a form of energy, the same equations for calculating the sensible heat gain to
1087 the air can be used to determine heat loss during expiration. Similarly, the caloric costs
1088 associated with the latent heat of vaporization will be the same values as the latent heat of
1089 condensation, just with a reversed sign. Thus, the equations used to determine the caloric costs of
1090 heating air during inspiration can be used to determine heat savings upon air cooling during
1091 expiration. The only change during expiration is the value for ΔH at the expired air temperature
1092 (cooler air holds less water), and the assumption that air leaves the nostril at 100% relative
1093 humidity regardless of expired air temperature [146].

1094 Energy savings were calculated by taking the calories returned to the body during air
1095 cooling and condensation during expiration and dividing it by the initial caloric cost of heating
1096 and humidifying the air during inspiration. Water saving were calculated following the method
1097 of Schmidt-Nielsen et al. [148].

1098 **Heat savings comparison with extant taxa**

1099 Comparison of the results from our two ankylosaur species to extant animals was
1100 accomplished by surveying the literature for data on heat and water savings within the nasal
1101 passages of extant birds, mammals, and reptiles (Tables 9–11). Direct data was available for the
1102 cactus wren (*Campylorhynchus brunneicapillus*) and kangaroo rat (*Dipodomys merriami*). [29]
1103 All other studies reported only the estimated water recovery from respiration. We manually
1104 calculated the heat savings for the remaining species based on estimates of inspired air during a
1105 single breath. These estimates were obtained from mass-dependent equations for tidal volume in

1106 mammals [149] and lizards [86]. Estimated caloric costs and estimated savings were calculated
 1107 using the methods described earlier (Tables 9 and 10).

1108 **Table 9. Taxa used for comparative energy savings graph**

Taxon	Reference
<i>Campylorhynchus brunneicapillus</i>	[29]
<i>Dipodomys merriami</i>	[29]
<i>Giraffa camelopardalis</i>	[33]
<i>Equus africanus</i>	[33]
<i>Dipsosaurus dorsalis</i>	[30]
<i>Corvus brachyrhynchos</i>	[38]
<i>Columba livia</i>	[38]

1109

1110 **Table 10. Inspiratory values for taxa studied**

Taxon	Tidal volume (ml)	Mass of air (g)	Heat capacity (cal/°C)	Temperature increase (°C)*	Total energy (cal)
<i>Giraffa Camelopardalis</i> [33]	5,959	6.78	1.63	16.2	26.4
<i>Equus africanus</i> [33]	1,605	1.82	0.44	14	6.16
<i>Dipsosaurus dorsalis</i> [30]	0.457	5.12e ⁻⁴	1.23e ⁻⁴	12	1.5e ⁻³
<i>Corvus brachyrhynchos</i> [38]	7.25*	8.14e ⁻³	1.95e ⁻³	26.1	5.1e ⁻²
<i>Columba livia</i> [38]	5.24*	5.90e ⁻³	1.41e ⁻³	25.7	3.6e ⁻²

1111

1112 **Table 11. Heat energy savings among taxa studied**

Taxon	Expired temp (°C)*	Mass of air (g)	Heat capacity (cal/°C)	Temp decrease (°C)	Energy saved (cal)
<i>Giraffa Camelopardalis</i> [33]	28.0	6.98	1.7	9.3	15.8
<i>Equus africanus</i> [33]	32.3	1.86	0.45	5.3	2.4
<i>Dipsosaurus dorsalis</i> [30]	35	5.24e ⁻⁴	1.3e ⁻⁴	7	9.1e ⁻⁴
<i>Corvus brachyrhynchos</i> [38]	21.9	8.68e ⁻³	2.1e ⁻³	19.2	4.0e ⁻²
<i>Columba livia</i> [38]	21.4	6.28e ⁻³	1.5e ⁻³	19.3	3.0e ⁻²

1113

1114 The results produced from this method provide a rough, “ballpark” comparison between
 1115 taxa. They allowed us to see the overall energy recovery capacity within the nasal passages.

1116 However, since these data came from three different studies with different protocols, these

1117 comparative results should not be viewed as equivalent. For instance, the study on the desert
1118 iguana (currently the only reptile to have such a study done) had measurements of inspiration
1119 and expiration at a variety of body temperatures [30]. To make the results from that paper more
1120 comparable to the mammal and bird data, we took the largest exhaled temperature drop
1121 observed, which was 7°C when the animal had a body temperature of 42°C in an ambient
1122 temperature of 30°C (note: Murrish and Schmidt-Nielsen [30] had a typographical error in their
1123 discussion that stated their lizards reduced air temperature by only 5°C. However, their results
1124 section and graphs indicate that 7°C is the correct number). Further, the authors did not test their
1125 lizards at an ambient temperature of 15°C, nor a relative humidity of 50%, thus making direct
1126 comparisons with Langman et al. [33] and Geist [38] impossible. Similarly, the data from
1127 Schmidt-Nielsen et al. [29] were for animals breathing in air at 25% relative humidity, whereas
1128 the data from Langman et al. [33] did not specify humidity, nor did they test at air temperatures
1129 of 15°C. Of the data used for comparisons, the data from Geist [38] are the most equivalent for
1130 comparison with our dinosaur models.

1131 **Validation Study**

1132 Prior to running our analysis on the ankylosaur models, we sought first to validate our
1133 methodology using empirically obtained data on heat transfer in pigeons [38]. We used CT data
1134 from a large adult domestic pigeon (*Columba livia*) and followed the methodology outlined
1135 above to simulate heat transfer within the nasal passage (Table 1, Fig. 3). As with the
1136 ankylosaurs, we only modeled heat transfer through the left nasal passage. Data obtained during
1137 inspiration were used to inform the expiration model under the assumption that warming of the
1138 air by the nasal walls came at the expense of an equal reduction in mucosal wall temperature.

1139 Environmental temperature and humidity were set to 15°C and 50% relative humidity,
1140 respectively, reflecting the conditions used by Geist [38].

1141 **Acknowledgments**

1142 We would like to thank the National Science Foundation (NSF) Graduate Research
1143 Fellowship to JMB. The Doris O. and Samuel P. Welles Research Fund and Jurassic Foundation
1144 for funding to JMB and WRP, as well as NSF grants (IBN-0343744, IOB-0517257, IOS-
1145 1050154, IOS-1456503) to LMW. Thanks to C. Mehling and M. Norell for loan of AMNH
1146 material. Thanks to D. Evans and K. Seymour for access to ROM material. For assistance with
1147 CT scanning of ankylosaur fossils, we thank H. Rockhold, RT, and OhioHealth O’Bleness
1148 Hospital, Athens, Ohio. Thanks to B. Van Valkenburgh and B. A. Craven for discussions on
1149 turbinate anatomy and general CFD questions. Thanks to R. Ridgely for initial segmentation and
1150 help with CT interpretation. Thanks to A. Morhardt, D. Cerio, and C. Early for useful
1151 discussions. Thanks to T. Miyashita and M.E. Burns for useful advice and critique on the
1152 manuscript.

1153

1154 **References**

- 1155 1. Vickaryous MK, Maryanska T, Weishampel DB. Ankylosauria. In: Weishampel DB,
1156 Dodson P, Osmolska H, editors. The Dinosauria. 2nd ed. Berkeley: University of
1157 California Press; 2004. pp. 363–392.
- 1158 2. Coombs WPJ. The Ankylosauria. Columbia University. 1971.
- 1159 3. Vickaryous MK, Russell AP, Currie PJ. Cranial ornamentation of ankylosaurs
1160 (Ornithischia: Thyreophora): Reappraisal of developmental hypotheses. In: Carpenter K,
1161 editor. The Armored Dinosaurs. Indianaopolis: Indiana University Press; 2001. pp. 318–
1162 340.
- 1163 4. Scheyer TM, Sander PM. Histology of ankylosaur osteoderms: implications for
1164 systematics and function. J Vertebr Paleontol. 2004;24: 874–893. doi:10.1671/0272-
1165 4634(2004)024[0874:HOAOIF]2.0.CO;2
- 1166 5. Main RP, de Ricqlès A, Horner JR, Padian K. The evolution and function of thyreophoran
1167 dinosaur scutes: implications for plate function in stegosaurs. Paleobiology. 2005;31: 291–
1168 314. doi:10.1666/0094-8373(2005)031[0291:TEAFOT]2.0.CO;2
- 1169 6. Hayashi S, Carpenter K, Scheyer TM, Watabe M, Suzuki D. Function and Evolution of
1170 Ankylosaur Dermal Armor. Acta Palaeontol Pol. 2010;55: 213–228.
1171 doi:10.4202/app.2009.0103
- 1172 7. Vickaryous MK, Sire JY. The integumentary skeleton of tetrapods: Origin, evolution, and
1173 development. J Anat. 2009;214: 441–464. doi:10.1111/j.1469-7580.2008.01043.x
- 1174 8. Coombs WPJ. The Bony Eyelid of *Euoplocephalus* (Reptilia , Ornithischia). J Paleontol.
1175 1972;46: 637–650.
- 1176 9. Maryańska T. New data on the skull of *Pinacosaurus grangeri* (Ankylosauria). Paleontol

- 1177 Pol. 1971;25: 45–53.
- 1178 10. Maryanska T. Ankylosauridae (Dinosauria) from Mongolia. *Palaeontol Pol.* 1977;37: 85–
1179 151. Available: http://www.palaeontologia.pan.pl/Archive/1977-37_85-151_19-36.pdf
- 1180 11. Brown B. The Ankylosauridae, a new family of armored dinosaurs from the Upper
1181 Cretaceous. *Bull Am Museum Nat Hist.* 1908;24: 187–201.
- 1182 12. Coombs WPJ. The families of the ornithischian dinosaur order Ankylosauria.
1183 *Paleontology.* 1978;21: 143–170.
- 1184 13. Coombs WPJ, Maryńska T. Ankylosauria. In: Weishampel DB, Dodson P, Osmólska H,
1185 editors. *The Dinosauria*. 1st ed. Berkeley: University of California Press; 1990. pp. 456–
1186 483.
- 1187 14. Witmer LM. The Evolution of the Antorbital Cavity of Archosaurs: A Study in Soft-
1188 Tissue Reconstruction in the Fossil Record with an Analysis of the Function of
1189 Pneumaticity. *J Vertebr Paleontol.* 1997;17: 1–76. doi:10.1080/02724634.1997.10011027
- 1190 15. Osmólska H. Nasal salt gland in dinosaurs. *Acta Palaeontol Pol.* 1979;24: 205–215.
- 1191 16. Hill R V., Witmer LM, Norell MA. A new specimen of *Pinacosaurus grangeri*
1192 (Dinosauria: Ornithischia) from the Late Cretaceous of Mongolia: Ontogeny and
1193 phylogeny of ankylosaurs. *Am Museum Novit.* 2003; 1–29. doi:10.1206/0003-
1194 0082(2003)395<0001:ANSOPG>2.0.CO;2
- 1195 17. Vickaryous MK, Russell AP. A redescription of the skull of *Euoplocephalus tutus*
1196 (Archosauria: Ornithischia): A foundation for comparative and systematic studies of
1197 ankylosaurian dinosaurs. *Zool J Linn Soc.* 2003;137: 157–186. doi:10.1046/j.1096-
1198 3642.2003.00045.x
- 1199 18. Carpenter K. Redescription of *Ankylosaurus magniventris* Brown 1908 (Ankylosauridae)

- 1200 from the Upper Cretaceous of the Western Interior of North America. *Can J Earth Sci.*
1201 2004;41: 961–986. doi:10.1139/e04-043
- 1202 19. Vickaryous MK. New information on the cranial anatomy of *Edmontonia rugosidens*
1203 Gilmore, a Late Cretaceous nodosaurid dinosaur from Dinosaur Provincial Park, Alberta. *J*
1204 *Vertebr Paleontol.* 2006;26: 1011–1013. doi:10.1671/0272-
1205 4634(2006)26[1011:NIOTCA]2.0.CO;2
- 1206 20. Witmer LM, Ridgely RC. The paranasal air sinuses of predatory and armored dinosaurs
1207 (Archosauria: Theropoda and Ankylosauria) and their contribution to cephalic structure.
1208 *Anat Rec.* 2008;291: 1362–1388. doi:10.1002/ar.20794
- 1209 21. Miyashita T, Arbour VM, Witmer LM, Currie PJ. The internal cranial morphology of an
1210 armoured dinosaur *Euoplocephalus* corroborated by X-ray computed tomographic
1211 reconstruction. *J Anat.* 2011;219: 661–675. doi:10.1111/j.1469-7580.2011.01427.x
- 1212 22. Kierszenbaum AL. Respiratory System. In: Kierszenbaum AL, editor. *Histology and Cell*
1213 *Biology: An Introduction to Pathology.* 2nd ed. Philadelphia: Elsevier; 2007. p. 437.
- 1214 23. Weldon PJ, Ferguson MWJ. Chemoreception in crocodylians - Anatomy, natural-history,
1215 and empirical results. *Brain Behav Evol.* 1993;41: 239–245. Available:
1216 isi:A1993KX56700018
- 1217 24. Craven BA, Neuberger T, Paterson EG, Webb AG, Josephson EM, Morrison EE, et al.
1218 Reconstruction and morphometric analysis of the nasal airway of the dog (*Canis*
1219 *familiaris*) and implications regarding olfactory airflow. *Anat Rec.* 2007;290: 1325–1340.
1220 doi:10.1002/ar.20592
- 1221 25. Martin BGH, Bellairs ADA. The narial excrescence and pterygoid bulla of the gharial,
1222 *Gavialis gangeticus* (Crocodylia). *J Zool.* 1977;182: 541–558. doi:10.1111/j.1469-

- 1223 7998.1977.tb04169.x
- 1224 26. Frey R, Volodin I, Volodina E. A nose that roars: Anatomical specializations and
1225 behavioural features of rutting male saiga. *J Anat.* 2007;211: 717–736.
1226 doi:10.1111/j.1469-7580.2007.00818.x
- 1227 27. Dinets V. Long-distance Signaling in Crocodylia. *Copeia.* 2013;2013: 517–526.
1228 doi:10.1643/CE-12-125
- 1229 28. Jackson DC, Schmidt-Nielsen K. Countercurrent heat exchange in the respiratory
1230 passages. *Proc Natl Acad Sci.* 1964;51: 1192–1197.
- 1231 29. Schmidt-Nielsen K, Hainsworth FR, Murrish DE. Counter-current heat exchange in the
1232 respiratory passages: Effect on water and heat balance. *Respir Physiol.* 1970;9: 263–276.
1233 doi:10.1016/0034-5687(70)90075-7
- 1234 30. Murrish DE, Schmidt-Nielsen K. Exhaled air temperature and wWater conservation in
1235 lizards. *Respir Physiol.* 1970;10: 151-. doi:10.1016/0034-5687(70)90079-4
- 1236 31. Collins JC, Pilkington TC, Schmidt-Nielsen K. A model of respiratory heat transfer in a
1237 small mammal. *Biophys J.* 1971;11: 886–914. doi:10.1016/S0006-3495(71)86262-8
- 1238 32. Murrish DE. Respiratory heat and water exchange in penguins. *Respir Physiol.* 1973;19:
1239 262–270. doi:10.1016/0034-5687(73)90030-3
- 1240 33. Langman VA, Maloiy GMO, Schmidt-Nielsen K, Schroter RC. Nasal heat exchange in the
1241 giraffe and other large mammals. *Respir Physiol.* 1979;37: 325–333. doi:10.1016/0034-
1242 5687(79)90079-3
- 1243 34. Hillenius WJ. The evolution of nasal turbinates and mammalian endothermy.
1244 *Paleobiology.* 1992;18: 17–29. doi:10.1017/S0094837300012197
- 1245 35. Hillenius WJ. Turbinates in therapsids: evidence for Late Permian origins of mammalian

1246 endothermy. *Evolution* (N Y). 1994;48: 207–229.

1247 36. Ruben JA, Hillenius WJ, Geist NR, Leitch A, Terry D, Currie PJ, et al. The metabolic
1248 status of Some Late Cretaceous Dinosaurs Source : *Science* , New Series , Vol . 273 , No .
1249 5279 (Aug . 30 , 1996) , pp . 1204-1207

1250 37. Ruben JA, Jones TD, Geist NR. Respiratory physiology of the dinosaurs. *BioEssays*.
1251 1998;20: 852–859. doi:10.1002/(SICI)1521-1878(199810)20:10<852::AID-
1252 BIES11>3.3.CO;2-H

1253 38. Geist NR. Nasal respiratory turbinate function in birds. *Physiol Biochem Zool*. 2000;73:
1254 581–589. doi:10.1086/317750

1255 39. Hillenius WJ, Ruben JA. The evolution of endothermy in terrestrial vertebrates: Who?
1256 When? Why? *Physiol Biochem Zool*. 2004;77: 1019–1042. doi:10.1086/425185

1257 40. Luckring JM, Rizzi A, Davis MB. Toward improved CFD predictions of slender airframe
1258 aerodynamics using the F-16XL aircraft (CAWAPI-2). *AIAA*. 2014;419: 1–14.

1259 41. Katz J. Aerodynamics of race cars. 2006; doi:10.1146/annurev.fluid.38.050304.092016

1260 42. Yam R, Yuen PL, Yung R, Choy T. Rethinking hospital general ward ventilation design
1261 using computational fluid dynamics. *J Hosp Infect*. Elsevier Ltd; 2011;77: 31–36.
1262 doi:10.1016/j.jhin.2010.08.010

1263 43. Hoi Y, Meng H, Woodward SH, Bendok BR, Hanel RA, Guterman LR, et al. Effects of
1264 arterial geometry on aneurysm growth: three- dimensional computational fluid dynamics
1265 study. *J Neurosurg*. 2004;101: 676–681.

1266 44. Chen XB, Lee HP, Fook V, Chong H, Wang DY. Assessment of septal deviation effects
1267 on nasal air flow : A computational fluid dynamics model. 2009; 1730–1736.
1268 doi:10.1002/lary.20585

- 1269 45. Craven BA, Paterson EG, Settles GS, Lawson MJ. Development and verification of a
1270 high-fidelity computational Fluid Dynamics model of canine nasal. 2009;131: 1–11.
1271 doi:10.1115/1.3148202
- 1272 46. Eiting TP, Smith TD, Perot JB, Dumont ER. The role of the olfactory recess in olfactory
1273 airflow. *J Exp Biol.* 2014;217: 1799–803. doi:10.1242/jeb.097402
- 1274 47. Kimbell JS, Godo MN, Gross E a, Joyner DR, Richardson RB, Morgan KT. Computer
1275 simulation of inspiratory airflow in all regions of the F344 rat nasal passages. *Toxicol*
1276 *Appl Pharmacol.* 1997;145: 388–398. doi:10.1006/taap.1997.8206
- 1277 48. Craven B a, Paterson EG, Settles GS. The fluid dynamics of canine olfaction: unique nasal
1278 airflow patterns as an explanation of macrosmia. *J R Soc Interface.* 2009;7: 933–43.
1279 doi:10.1098/rsif.2009.0490
- 1280 49. Frappell PB, Hinds DS, Boggs DF. Scaling of respiratory variables and the breathing
1281 pattern in birds: An allometric and phylogenetic approach. *Physiol Biochem Zool.*
1282 2001;74: 75–89. doi:10.1086/319300
- 1283 50. Farmer CG. On the origin of avian air sacs. *Respir Physiol Neurobiol.* 2006;154: 89–106.
1284 doi:10.1016/j.resp.2006.04.014
- 1285 51. Eagle RA, Tutken T, Martin TS, Tripathi AK, Fricke HC, Connely M, et al. Dinosaur body
1286 temperatures Determined from isotopic (¹³C-¹⁸O) Ordering in Fossil Biominerals.
1287 *Science (80-).* 2011;333: 443–445. doi:10.1126/science.1206196
- 1288 52. Eagle RA, Enriquez M, Grellet-Tinner G, Perez-Huerta A, Hu D, Tutken T, et al. Isotopic
1289 ordering in eggshells reflects body temperatures and suggests differing thermophysiology
1290 in two Cretaceous dinosaurs. *Nat Commun.* 2015;6: 8296. doi:10.1038/ncomms9296
- 1291 53. Kinahan AA, Inge-moller R, Bateman PW, Kotze A, Scantlebury M. Body temperature

- 1292 daily rhythm adaptations in African savanna elephants (*Loxodonta africana*). *Physiol*
1293 *Behav.* 2007;92: 560–565. doi:10.1016/j.physbeh.2007.05.001
- 1294 54. Phillipis PK, Heath JE. Dependency of surface temperature regulation on body size in
1295 terrestrial mammals. *J Therm Biol.* 1995;20: 281–289.
- 1296 55. Weissenböck NM, Arnold W, Ruf T. Taking the heat: Thermoregulation in Asian
1297 elephants under different climatic conditions. *J Comp Physiol B Biochem Syst Environ*
1298 *Physiol.* 2012;182: 311–319. doi:10.1007/s00360-011-0609-8
- 1299 56. Rowe MF, Bakken GS, Ratliff JJ, Langman V a. Heat storage in Asian elephants during
1300 submaximal exercise: Behavioral regulation of thermoregulatory constraints on activity in
1301 endothermic gigantotherms. *J Exp Biol.* 2013;216: 1774–85. doi:10.1242/jeb.076521
- 1302 57. Langman VA. Heat balance in the black rhinoceros (*Diceros bicornis*). *Natl Geogr Res*
1303 *Reports.* 1985;21: 251–254.
- 1304 58. Kock M, Grange M la, Toit R du. Chemical immobilization of Free-ranging black
1305 rhinoceros (*Diceros bicornis*) using combinations of etorphine (M99), Fentanyl, and
1306 xylazine. *J Zoo Wildl Med.* 1990;21: 155–165.
- 1307 59. Allbrook DB, Harthoorn AM, Luck CP, Wright PG. Temperature regulation in the white
1308 rhinoceros. *J Physiol.* 1958;143: 51–52.
- 1309 60. Citino SB, Bush M. Reference cardiopulmonary physiologic parameters for standing,
1310 unrestrained white rhinoceroses (*Ceratotherium simum*). *J Zoo Wildl Med.* 2007;38: 375–
1311 9. doi:10.1638/2006-0007R1.1
- 1312 61. Bligh J, Harthoorn AM. Continuous radiotelemetric records of the deep body temperature
1313 of some unrestrained African mammals under near-natural conditions. *J Physiol.*
1314 1965;176: 145–162.

- 1315 62. Langman VA, Bamford OS, Maloiy GMO. Respiration and metabolism in the giraffe.
1316 Respir Physiol. 1982;50: 141–152. doi:10.1016/0034-5687(82)90013-5
- 1317 63. Schwartz CC, Miller SD, Haroldson MA. Grizzly Bear. In: Feldhamer GA, Thompson
1318 BC, Chapman JA, editors. Wild Mammals of North America: Biology, Management, and
1319 Conservation. 2nd ed. Baltimore: Johns Hopkins University Press; 2003. pp. 556–586.
- 1320 64. Prinzinger R, Preßmar A, Schleucher E. Body temperature in birds. Comp Biochem
1321 Physiol. 1991;99: 499–506.
- 1322 65. Maloney SK, Dawson TJ. Sexual dimorphism in basal metabolism and body temperature
1323 of a large bird, the emu. Condor. 1993;95: 1034–1037.
- 1324 66. Bligh J, Hartley TC. The deep body temperature of an unrestrained ostrich *Struthio*
1325 *camelus* recorded continuously by a radio-telemetric technique. Ibis (Lond 1859).
1326 1965;107: 104–105.
- 1327 67. Mackay RS. Galapagos tortoise and marine iguana deep body temperature measured by
1328 radio telemetry. Nature. 1964;204: 355–358.
- 1329 68. McNab BK, Auffenberg W. The effect of large body size on the temperature regulation of
1330 the komodo dragon, *Varanus komodoensis*. Comp Biochem Physiol Part A Physiol.
1331 1976;55: 345–350. doi:10.1016/0300-9629(76)90058-X
- 1332 69. Michaeli G, Pinshow B. Respiratory water loss in free-flying pigeons. J Exp Biol.
1333 2001;204: 3803–3814.
- 1334 70. Naftali S, Rosenfeld M, Wolf M, Elad D. The air-conditioning capacity of the human
1335 nose. Ann Biomed Eng. 2005;33: 545–553. doi:10.1007/s10439-005-2513-4
- 1336 71. Vogel S. Life in Moving Fluids. 2nd ed. Princeton: Princeton University Press; 1994.
- 1337 72. Porter WR. Physiological implications of dinosaur cephalic vascular systems. Ohio

- 1338 University. 2015.
- 1339 73. Brown CM, Evans DC, Campione NE, O'Brien LJ, Eberth DA. Evidence for taphonomic
1340 size bias in the Dinosaur Park Formation (Campanian, Alberta), a model Mesozoic
1341 terrestrial alluvial-paralic system. *Palaeogeogr Palaeoclimatol Palaeoecol.* Elsevier B.V.;
1342 2013;372: 108–122. doi:10.1016/j.palaeo.2012.06.027
- 1343 74. Mallon JC, Anderson JS. Implications of beak morphology for the evolutionary
1344 paleoecology of the megaherbivorous dinosaurs from the Dinosaur Park Formation (upper
1345 Campanian) of Alberta, Canada. *Palaeogeogr Palaeoclimatol Palaeoecol.* Elsevier B.V.;
1346 2014;394: 29–41. doi:10.1016/j.palaeo.2013.11.014
- 1347 75. Ósi A, Prondvai E, Mallon J, Bodor ER. Diversity and convergences in the evolution of
1348 feeding adaptations in ankylosaurs (Dinosauria: Ornithischia)*. *Hist Biol.* Taylor &
1349 Francis; 2017;29: 539–570. doi:10.1080/08912963.2016.1208194
- 1350 76. Brown CM, Evans DC, Campione NE, O'Brien LJ, Eberth DA. Evidence for taphonomic
1351 size bias in the Dinosaur Park Formation (Campanian, Alberta), a model Mesozoic
1352 terrestrial alluvial-paralic system. *Palaeogeogr Palaeoclimatol Palaeoecol.* Elsevier B.V.;
1353 2013;372: 108–122. doi:10.1016/j.palaeo.2012.06.027
- 1354 77. Schmidt-Nielsen K. *Scaling: Why is animal size so important?* Cambridge: Cambridge
1355 University Press; 1984.
- 1356 78. Arbour VM, Mallon JC. Unusual cranial and postcranial anatomy in the archetypal
1357 ankylosaur *Ankylosaurus magniventris*. 2017; 764–794. doi:10.1139/facets-2017-0063
- 1358 79. Paul GS. *The Princeton Field Guide to Dinosaurs*. 2nd ed. Paul GS, editor. Princeton:
1359 Princeton University Press; 2016.
- 1360 80. Leahey LG, Molnar RE, Carpenter K, Witmer LM, Salisbury SW. Cranial osteology of

- 1361 the ankylosaurian dinosaur formerly known as *Minmi* sp. (Ornithischia: Thyreophora)
1362 from the Lower Cretaceous Allaru Mudstone of Richmond, Queensland, Australia. PeerJ.
1363 2015;3: e1475. doi:10.7717/peerj.1475
- 1364 81. Bourke JM, Porter WR, Ridgely RC, Lyson TR, Schachner ER, Bell PR, et al. Breathing
1365 life into dinosaurs: Tackling challenges of soft-tissue restoration and nasal airflow in
1366 extinct Species. *Anat Rec.* 2014;297: 2148–2186. doi:10.1002/ar.23046
- 1367 82. Owerkowicz T, Musinsky C, Middleton KM, Crompton AW. Respiratory turbinates and
1368 the evolution of endothermy in mammals and birds. In: Dial KP, Shubin NH, Brainerd EL,
1369 editors. *Great Transformations in Vertebrate Evolution*. Chicago: University of Chicago
1370 Press; 2015. pp. 143–165.
- 1371 83. Bourke JM, Witmer LM. Nasal conchae function as aerodynamic baffles: Experimental
1372 computational fluid dynamic analysis in a turkey nose (Aves: Galliformes). *Respir Physiol*
1373 *Neurobiol.* Elsevier B.V.; 2016;234: 32–46. doi:10.1016/j.resp.2016.09.005
- 1374 84. Van Valkenburgh B, Theodor J, Friscia A, Pollack A, Rowe T. Respiratory turbinates of
1375 canids and felids: a quantitative comparison. *J Zool.* 2004;264: 281–293.
1376 doi:10.1017/s0952836904005771
- 1377 85. Stebbins RC. Nasal structure in lizards with reference to olfaction and conditioning of the
1378 inspired air. *Am J Anat.* 1948;83: 183–221. doi:10.1002/aja.1000830202
- 1379 86. Bennett AF. Ventilation in two species of lizards during rest and activity. *Comp Biochem*
1380 *Physiol -- Part A Physiol.* 1973;46: 653–671. doi:10.1016/0300-9629(73)90119-9
- 1381 87. O'Connor PM, Claessens LP a M. Basic avian pulmonary design and flow-through
1382 ventilation in non-avian theropod dinosaurs. *Nature.* 2005;436: 253–256.
1383 doi:10.1038/nature03716

- 1384 88. Wedel MJ. Vertebral pneumaticity, air sacs, and the physiology of sauropod dinosaurs.
1385 Paleobiology. 2003;29: 243–255. doi:10.1666/0094-
1386 8373(2003)029<0243:VPASAT>2.0.CO;2
- 1387 89. Farmer CG, Sanders K. Unidirectional airflow in the lungs of alligators. Science (80-).
1388 2010;327: 338–340. doi:10.1126/science.1180219
- 1389 90. Schachner ER, Hutchinson JR, Farmer C. Pulmonary anatomy in the Nile crocodile and
1390 the evolution of unidirectional airflow in Archosauria. PeerJ. 2013;1: e60.
1391 doi:10.7717/peerj.60
- 1392 91. Schachner ER, Cieri RL, Butler JP, Farmer CG. Unidirectional pulmonary airflow
1393 patterns in the savannah monitor lizard. Nature. Nature Publishing Group; 2014;506: 367–
1394 70. doi:10.1038/nature12871
- 1395 92. Porter WR, Witmer LM. Vascular Patterns in Iguanas and Other Squamates : Blood
1396 Vessels and Sites of Thermal Exchange. 2015; 1–27. doi:10.1371/journal.pone.0139215
- 1397 93. Porter WR, Sedlmayr JC, Witmer LM. Vascular patterns in the heads of crocodylians:
1398 blood vessels and sites of thermal exchange. J Anat. 2016;229: 800–824.
1399 doi:10.1111/joa.12539
- 1400 94. Porter WR, Witmer LM. Avian cephalic vascular anatomy, sites of thermal exchange, and
1401 the rete ophthalmicum. Anat Rec. 2016;299: 1461–1486. doi:10.1002/ar.23375
- 1402 95. Heath JE. Head-body temperature differences in horned lizards. Physiol Zool. 1964;37:
1403 273–279.
- 1404 96. Johnson CR. Thermoregulation in pythons-II. Head-body temperature differences and
1405 thermal preferenda in australian pythons. Comp Biochem Physiol -- Part A Physiol.
1406 1973;45: 1065–1087. doi:10.1016/0300-9629(73)90343-5

- 1407 97. Johnson CR. Thermoregulation in crocodylians-I. Head-body temperature control in the
1408 Papuan-New Guinean crocodiles, *Crocodylus novaeguineae* and *Crocodylus porosus*.
1409 Comp Biochem Physiol. 1974;49A: 3–28.
- 1410 98. Pough FH, McFarland WN. A physical basis for head-body temperature differences in
1411 reptiles. Comparative Biochemistry and Physiology -- Part A: Physiology. 1976. pp. 301–
1412 303. doi:10.1016/S0300-9629(76)80040-0
- 1413 99. Tattersall GJ, Cadena V, Skinner MC. Respiratory cooling and thermoregulatory coupling
1414 in reptiles. Respir Physiol Neurobiol. 2006;154: 302–318. doi:10.1016/j.resp.2006.02.011
- 1415 100. Baker MA, Chapman LW, Nathanson M. Control of Brain Temperature in Dogs: Effects
1416 of Tracheostomy. Respir Physiol. 1974;22: 325–333.
- 1417 101. Crawford EC, Palomeque J, Barber BJ. A physiological basis for head-body temperature
1418 differences in a panting lizard. Comparative Biochemistry and Physiology -- Part A:
1419 Physiology. 1977. pp. 161–163. doi:10.1016/0300-9629(77)90178-5
- 1420 102. Baker M a. Brain cooling in endotherms in heat and exercise. Annu Rev Physiol. 1982;44:
1421 85–96. doi:10.1146/annurev.ph.44.030182.000505
- 1422 103. Caputa M. Selective brain cooling: A multiple regulatory mechanism. J Therm Biol.
1423 2004;29: 691–702. doi:10.1016/j.jtherbio.2004.08.079
- 1424 104. Witmer LM, Ridgely RC, Dufeu DL, Semones MC. Using CT to peer into the past : 3D
1425 visualization of the brain and ear regions of birds, crocodiles, and nonavian dinosaurs.
1426 Anat Imaging. 2008; 33. doi:10.1007/978-4-431-76933-0
- 1427 105. Witmer LM, Sampson SD. Nasal Conchae and blood supply in some dinosaurs :
1428 Physiological implications narial novelty in dinosaurs. J Vertebr Paleontol 1999; 19
1429 (3 supp):85A

- 1430 106. Parsons TS. Nasal anatomy and the phylogeny of Reptiles. *Evolution* (N Y). 1959;13:
1431 175–187.
- 1432 107. Parsons TS. Evolution of the nasal structure in the lower tetrapods. *Integr Comp Biol*.
1433 1967;7: 397–413. doi:10.1093/icb/7.3.397
- 1434 108. Bang BG, Wenzel BM. Nasal cavity and olfactory system. *Form and Function in Birds*.
1435 2007. pp. 195–225.
- 1436 109. Witmer LM. Homology of facial structures in extant archosaurs (birds and crocodylians),
1437 with special reference to paranasal pneumaticity and nasal conchae. *J Morphol*. 1995;225:
1438 269–327. doi:10.1002/jmor.1052250304
- 1439 110. Leahey LG, Molnar RE, Carpenter K, Witmer LM, Salisbury SW. Cranial osteology of
1440 the ankylosaurian dinosaur formerly known as *Minmi* sp. (Ornithischia: Thyreophora)
1441 from the Lower Cretaceous Allaru Mudstone of Richmond, Queensland, Australia. *PeerJ*.
1442 2015;3: e1475. doi:10.7717/peerj.1475
- 1443 111. Parsons TS. Studies on the comparative embryology of the reptilian nose. *Bull Museum*
1444 *Comp Zool*. 1959;120: 101–277.
- 1445 112. Arbour VM, Currie PJ. *Euoplocephalus tutus* and the Diversity of Ankylosaurid
1446 Dinosaurs in the Late Cretaceous of Alberta, Canada, and Montana, USA. *PLoS One*.
1447 2013;8. doi:10.1371/journal.pone.0062421
- 1448 113. Witmer LM. Nostril position in dinosaurs and other vertebrates and its significance for
1449 nasal function. *Science* (80-). 2001;293: 850–3. doi:10.1126/science.1062681
- 1450 114. Jarvik E. On the structure of the snout of crossopterygians and lower gnathostomes in
1451 general. *Zool Bidr Upsala*. 1942;21: 235–675.
- 1452 115. Baumel J, Witmer L. *Osteologia. Handb Avian Anat Nomina Anat Avium*, 2nd Ed. 1993;

- 1453 45–131.
- 1454 116. Zusi RL, Livezey BC. Variation in the Os Palatinum and its structural relation to the
1455 Palatum Osseum of Birds (Aves). *Ann Carnegie Museum*. 2006;75: 137.
1456 doi:10.2992/0097-4463(2006)75[137:VITOPA]2.0.CO;2
- 1457 117. Crole MR, Soley JT. Gross morphology of the intra-oral rhamphotheca, oropharynx and
1458 proximal oesophagus of the emu (*Dromaius novaehollandiae*). *J Vet Med Ser C Anat*
1459 *Histol Embryol*. 2010;39: 207–218. doi:10.1111/j.1439-0264.2010.00998.x
- 1460 118. Parsons TS. The nose and Jacobson’s organ. In: Gans C, editor. *Biology of the Reptilia*
1461 *Volume 2*. New York: Academic Press; 1970. pp. 99–191.
- 1462 119. Rieppel O, Gauthier J, Maisano J. Comparative morphology of the dermal palate in
1463 squamate reptiles, with comments on phylogenetic implications. *Zool J Linn Soc*.
1464 2008;152: 131–152. doi:10.1111/j.1096-3642.2007.00337.x
- 1465 120. Witmer LM. The extant phylogenetic bracket and the importance of reconstructing soft
1466 tissues in Fossils. In: Thomason JJ, editor. *Functional Morphology in Vertebrate*
1467 *Paleontology*. New York: Cambridge University Press; 1995. pp. 19–33.
- 1468 121. Vickaryous MK. *Skull morphology of the Ankylosauria*. Library. The University of
1469 Calgary. 2001.
- 1470 122. Romer AS. *Osteology of the Reptiles*. Malabar: Krieger Publishing Company; 1956.
- 1471 123. Negus V. *The comparative anatomy and physiology of the nose and paranasal sinuses*.
1472 London: Livingstone; 1958.
- 1473 124. Cave AJE. The nature and function of the mammalian epipharynx. *J Zool Soc London*.
1474 1967;153: 277–289.
- 1475 125. Carpenter K. Ankylosaur systematics: Example using *Panoplosaurus* and *Edmontonia*

1476 (Ankylosauria: Nodosauridae). In: Carpenter K, Currie PJ, editors. Dinosaur Systematics
1477 Approaches and Perspectives. New York: Cambridge University Press; 1990. pp. 281–
1478 298.

1479 126. Schoenfeld TA, Cleland TA. The anatomical logic of smell. Trends Neurosci. 2005;28:
1480 620–627. doi:10.1016/j.tins.2005.09.005

1481 127. Lucas A, Douglas LC. Principles underlying ciliary activity in the respiratory tract. Arch
1482 Otolaryngol. 1934;20: 518–541.

1483 128. Winet H, Yates GT, Wu TY, Head J. On the mechanics of mucociliary flows . II . A
1484 fluorescent tracer method for obtaining flow velocity profiles in mucus. 1982;34: 29–34.

1485 129. Yerry MA, Shephard MS. Automatic three-dimensional mesh generation by the modified-
1486 OCTREE technique. Int J Numer Methods Eng. 1984;20: 1965–1990.

1487 130. Georges P, Hecht F, Saltel E. Constraint of the boundary and automatic mesh generation.
1488 In: Sengupta S, HäuserJ, Eiseman PR, Thompson JF, editors. Numerical Grid Generation
1489 in Computational Fluid Mechanics. Swansea: Pineridge; 1988. pp. 589–597.

1490 131. Shephard MS, Georges MK. Automatic three-dimensional mesh generation by the finite
1491 OCTREE technique. Int J Numer Methods Eng. 1991;32: 709–749.

1492 132. Biswas R, Strawn RC. Tetrahedral and hexahedral mesh adaptation for CFD Problems.
1493 Appl Numer Math. 1998;26: 135–151.

1494 133. Longest PW, Vinchurkar S. Effects of mesh style and grid convergence on particle
1495 deposition in bifurcating airway models with comparisons to experimental data. 2007;29:
1496 350–366. doi:10.1016/j.medengphy.2006.05.012

1497 134. Vogel S. Viscosity and the patterns of flow. In: Vogel S, editor. Comparative
1498 Biomechanics: Life’s Physical World. New Jersey: Princeton University Press; 2003. pp.

- 1499 117–138.
- 1500 135. Holmes WM, Cotton R, Xuan VB, Rygg AD, Craven BA, Abel RL, et al. Three-
1501 dimensional structure of the nasal passageway of a hagfish and its implications for
1502 olfaction. *Anat Rec.* 2011;294: 1045–1056. doi:10.1002/ar.21382
- 1503 136. Foss JF. Basic engineering fluid mechanics. *The Handbook of Fluid Dynamics*. Florida:
1504 CRC Press; 1998. pp. 5–1–5–9.
- 1505 137. Womersley JR. Method for the calculation of velocity, rate of flow and viscous drag in
1506 arteries when the pressure gradient is known. *J Physiol.* 1955;127: 553–563.
- 1507 138. Ku DN. Blood flow in arteries. *Annu Rev Fluid Mech.* 1997;29: 399–434.
1508 doi:10.1146/annurev.fluid.29.1.399
- 1509 139. Zhao K, Dalton P, Yang GC, Scherer PW. Numerical modeling of turbulent and laminar
1510 airflow and odorant transport during sniffing in the human and rat nose. *Chem Senses.*
1511 2006;31: 107–118. doi:10.1093/chemse/bjj008
- 1512 140. Horschler I, Brücker C, Schröder W, Meinke M. Investigation of the impact of the
1513 geometry on the nose flow. 2006;25: 471–490. doi:10.1016/j.euromechflu.2005.11.006
- 1514 141. Jiang J, Zhao K. Airflow and nanoparticle deposition in rat nose under various breathing
1515 and sniffing conditions — A computational evaluation of the unsteady and turbulent effect
1516 \$. *J Aerosol Sci.* Elsevier; 2010;41: 1030–1043. doi:10.1016/j.jaerosci.2010.06.005
- 1517 142. Wilcox DC. Multiscale model for turbulent flows. *AIAA J.* 1988;26: 1311–1320.
1518 doi:10.2514/3.10042
- 1519 143. Barrick RE, Fischer AG, Showers WJ. Oxygen isotopes from turtle bone: Applications for
1520 terrestrial paleoclimates? *Palaios.* 1999;14: 186–191. doi:10.2307/3515374
- 1521 144. Amiot R, Lecuyer C, Buffetaut E, Fluteau F, Legendre S, Martineau F. Latitudinal

1522 temperature gradient during the Cretaceous Upper Campanian-Middle Maastrichtian : δ
1523 ^{18}O record of continental vertebrates. *Earth Planet Sci Lett.* 2004;226: 255–272.
1524 doi:10.1016/j.epsl.2004.07.015

1525 145. Bourke JM. Implications of airflow dynamics and soft-tissue reconstruction for the heat
1526 exchange potential of dinosaur nasal passages. Ohio University. 2015.

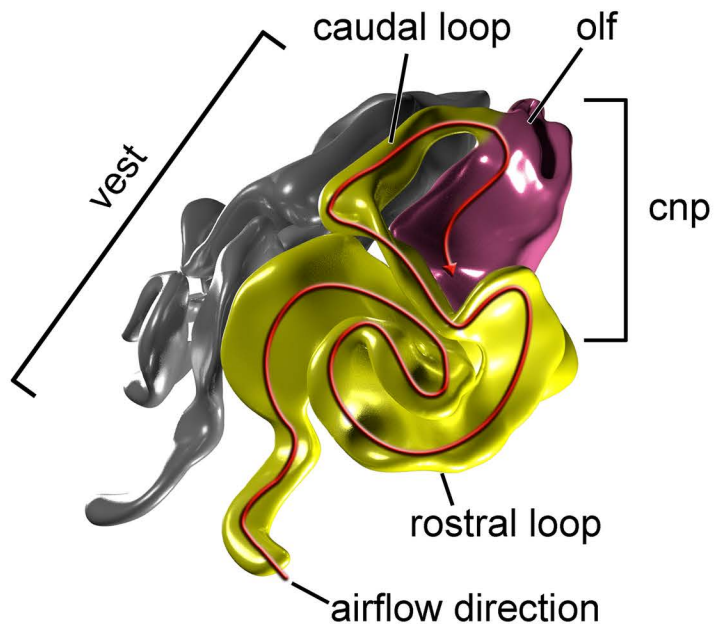
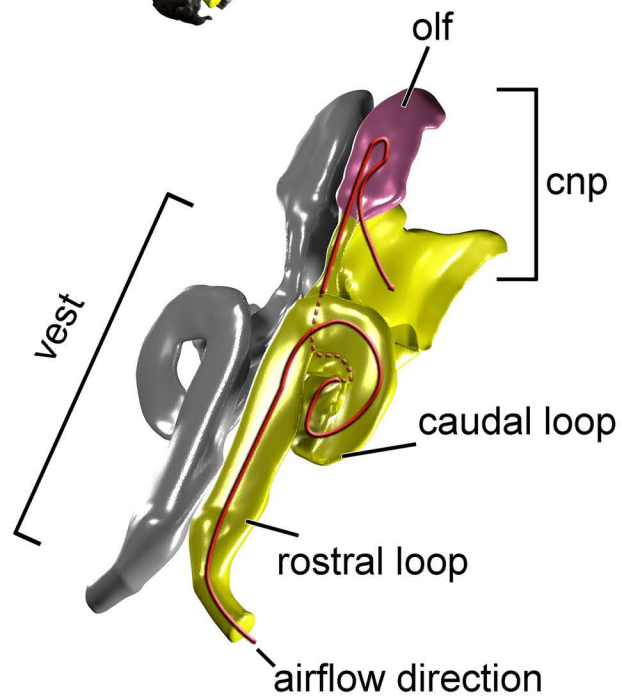
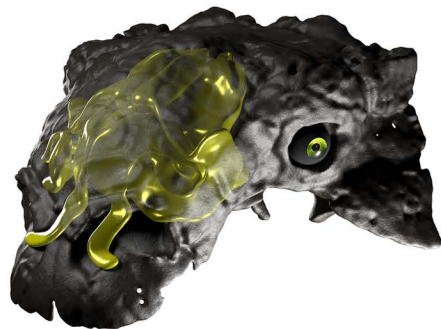
1527 146. Schmidt-Nielsen K. *Animal Physiology*. 5th ed. Schmidt-Nielsen K, editor. Cambridge:
1528 Cambridge University Press; 1997.

1529 147. Tu J, Yeoh G, Liu C. *Computational Fluid Dynamics*. 2nd ed. Tu J, Yeoh G, Liu C,
1530 editors. New York: Elsevier B.H.; 2013.

1531 148. Schmidt-Nielsen K, Schroter RC, Shkolnik A. Desaturation of exhaled air in camels. *Proc*
1532 *R Soc London Ser B Biol Sci.* 1981;211: 305–319. doi:10.1098/rspb.1981.0009

1533 149. Stahl WR. Scaling of respiratory variables in mammals. *J Appl Physiol.* 1967;22: 453–
1534 460.

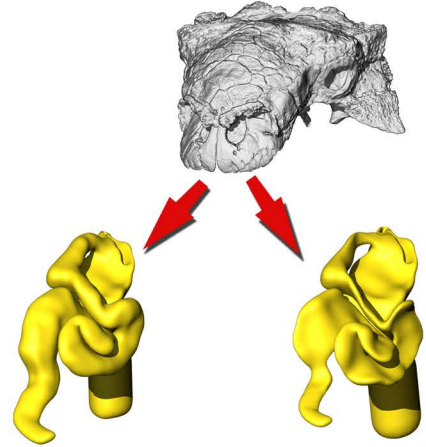
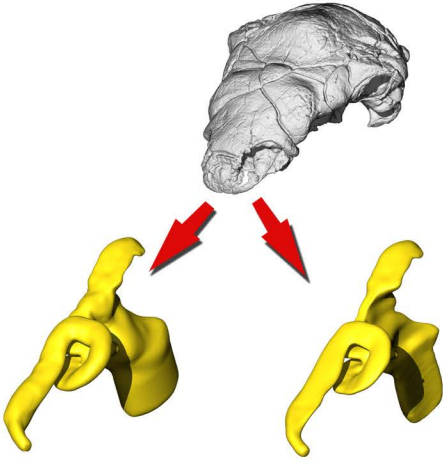
1535
1536

A**B**

Primary Analyses

Panoplosaurus

Euoplocephalus



BB airway

ST airway

BB airway

ST airway

Airway size limited by nasal cavity. Airflow based on mass-specific equation (high flow), or Reverse Reynolds approach (low flow). Inspiration and Expiration tested.

Airway size limited by diffusion. Guided by airway limits in extant animals. Airflow based on mass-specific equation (high flow) or Reverse Reynolds approach (low flow). Inspiration and Expiration tested.

Airway size limited by nasal cavity. Airflow based on mass-specific equation (high flow), or Reverse Reynolds approach (low flow). Inspiration and Expiration tested.

Airway size limited by diffusion. Guided by airway limits in extant animals. Airflow based on mass-specific equation (high flow) or Reverse Reynolds approach (low flow). Inspiration and Expiration tested.

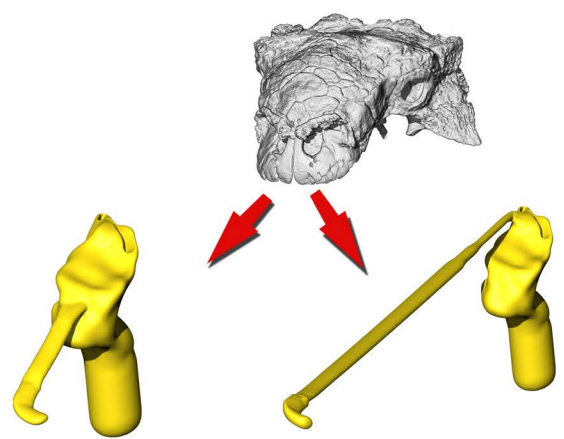
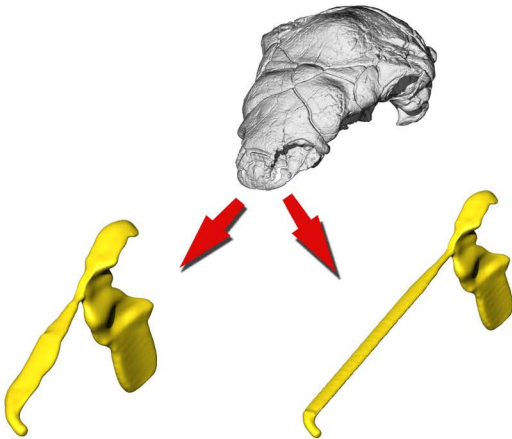
A

B

C

D

Secondary Analyses



Basic

Straightened

Basic

Straightened

ST airway model modified. Nasal vestibule shortened to minimum length from nostril to CNP. Reverse-Reynolds airflow (low flow) used to enhance heat transfer capability.

ST airway model modified. Nasal vestibule length maintained, but convolutions have been removed. Reverse-Reynolds airflow (low flow) used to enhance heat transfer capability.

ST airway model modified. Nasal vestibule shortened to minimum length from nostril to CNP. Reverse-Reynolds airflow (low flow) used to enhance heat transfer capability.

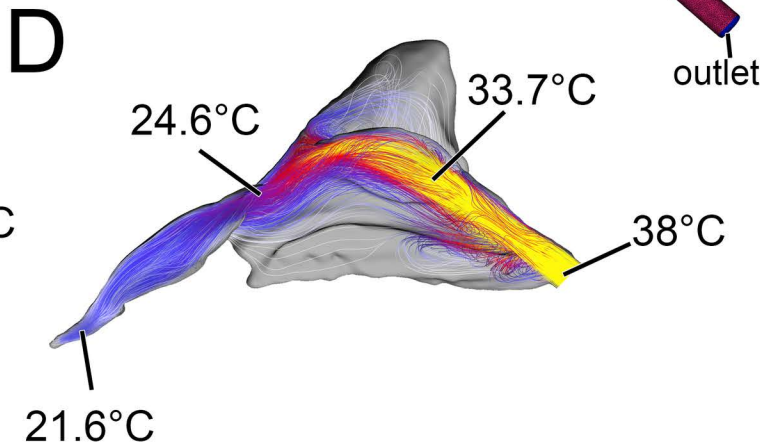
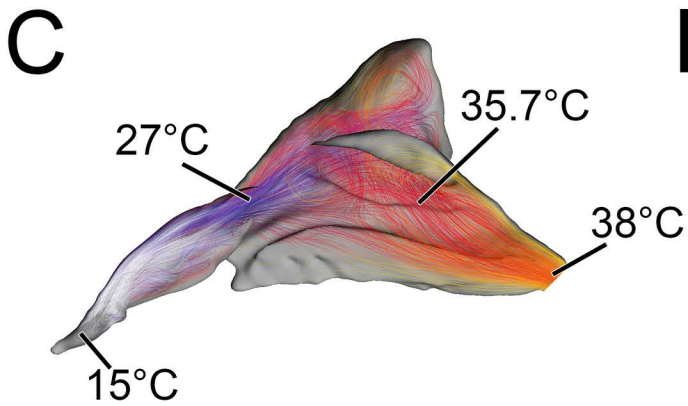
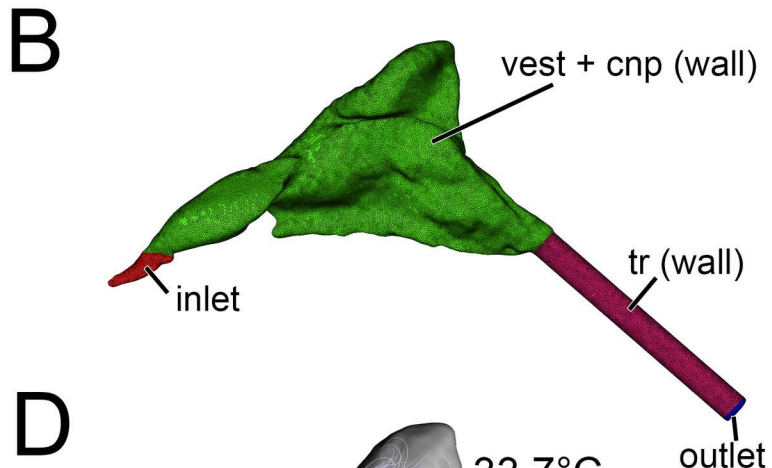
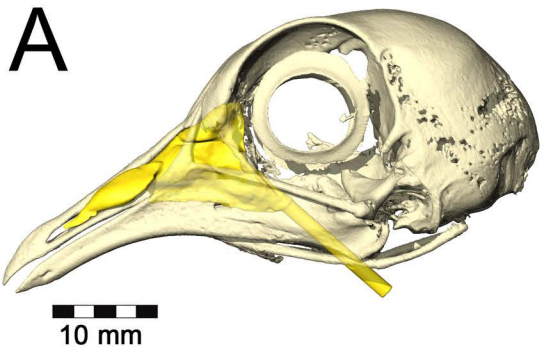
ST airway model modified. Nasal vestibule length maintained, but convolutions have been removed. Reverse-Reynolds airflow (low flow) used to enhance heat transfer capability.

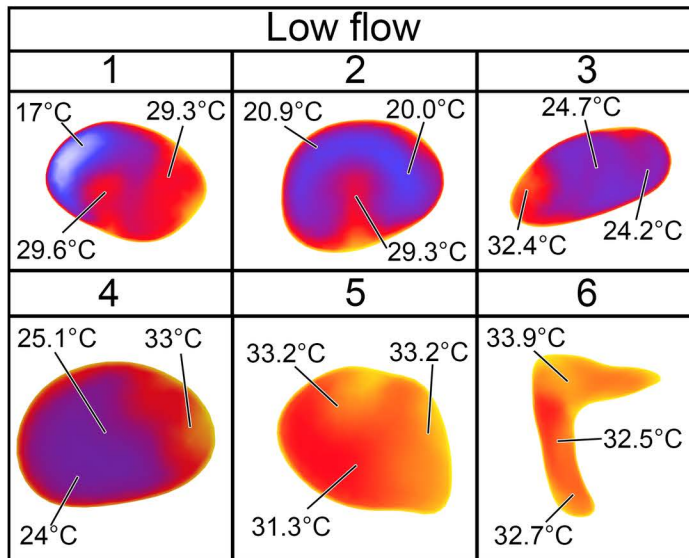
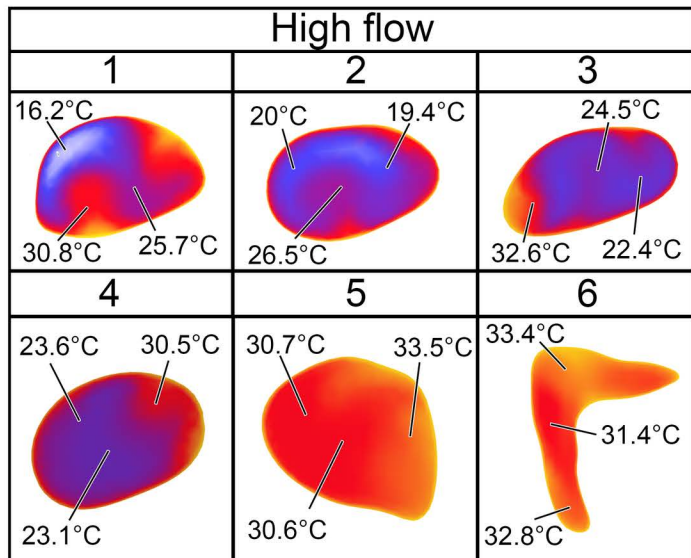
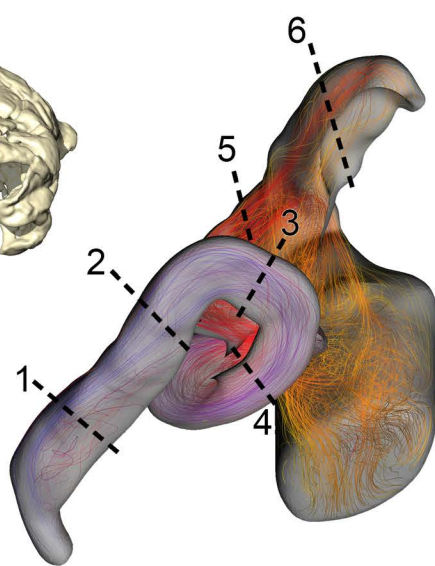
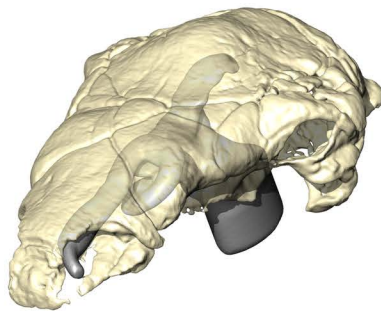
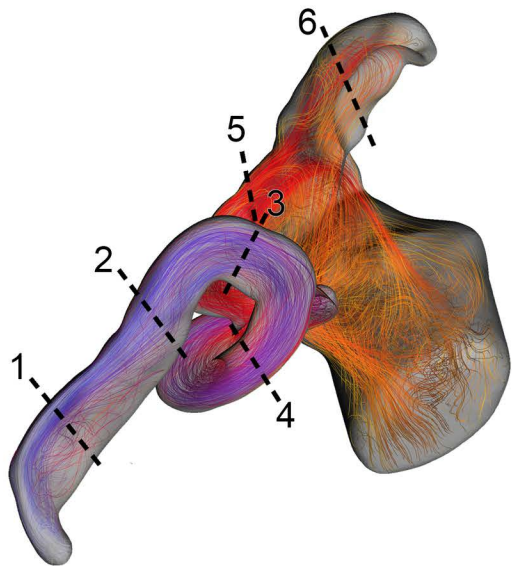
E

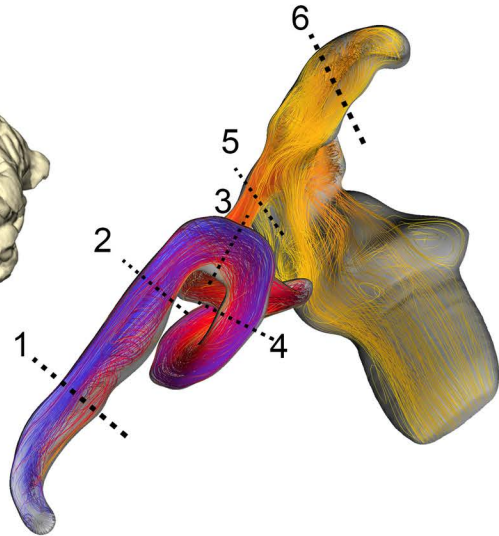
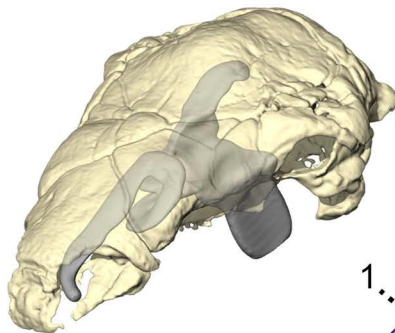
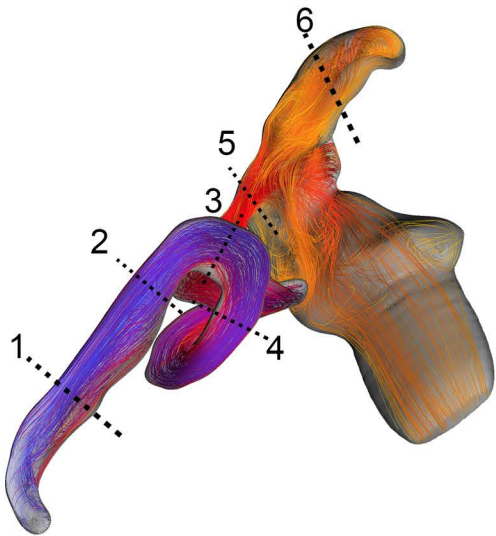
F

G

H

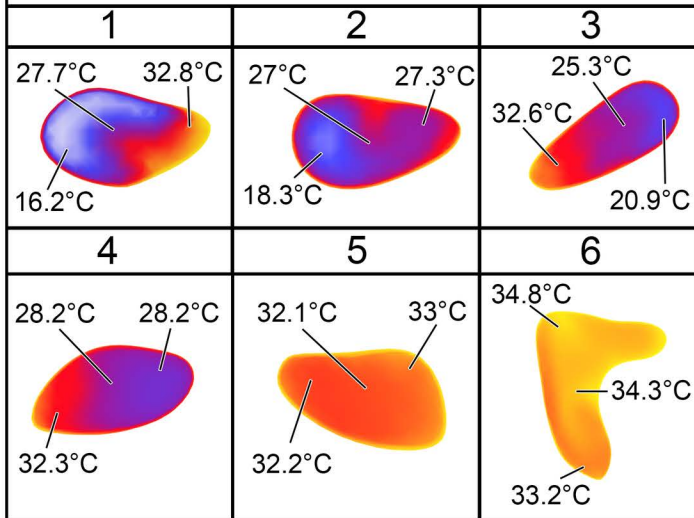
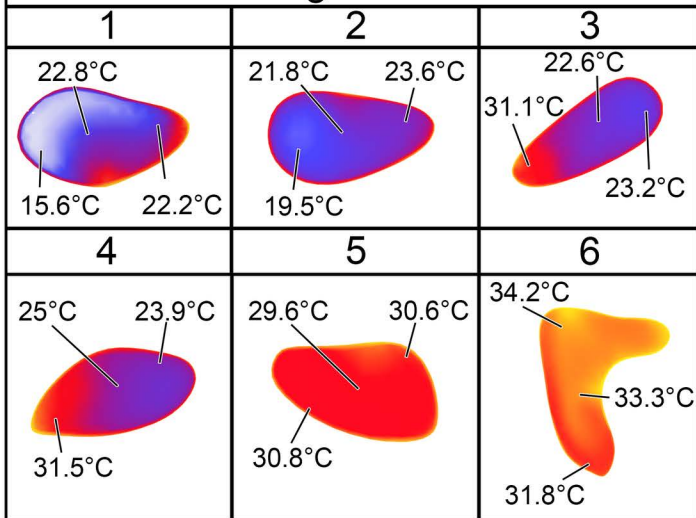


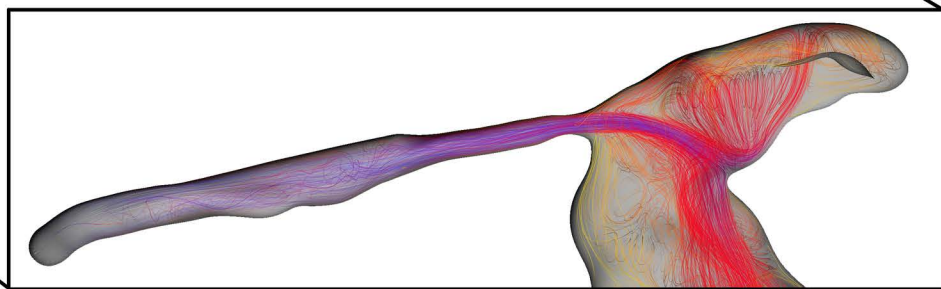
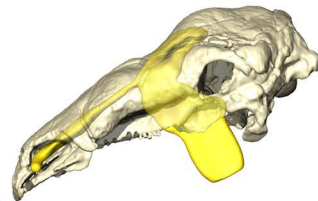
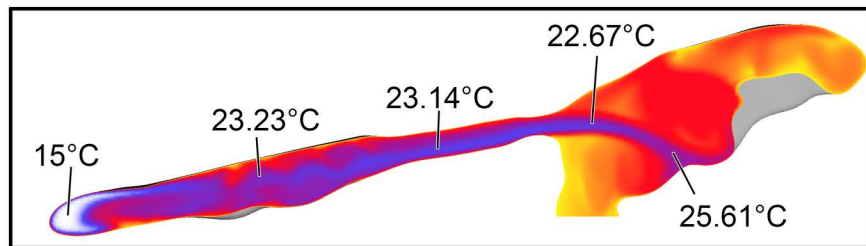




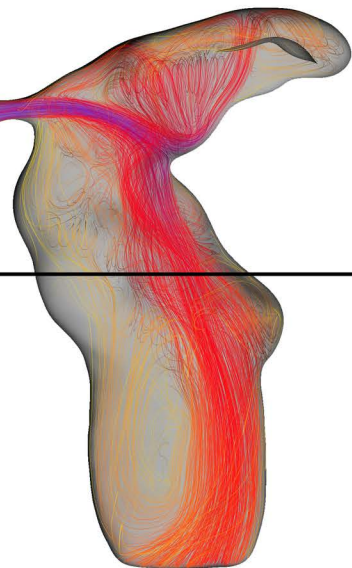
High flow

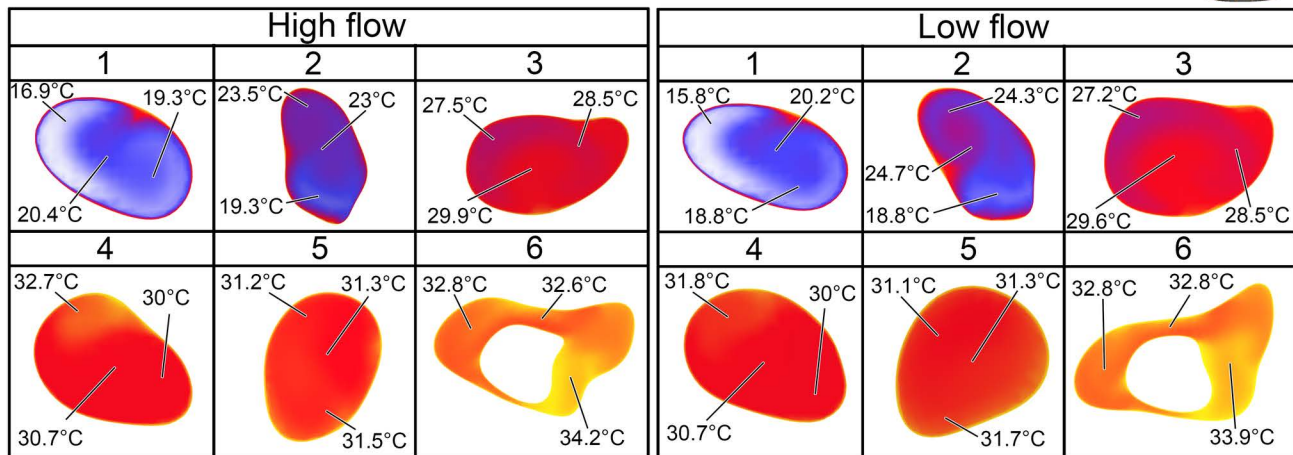
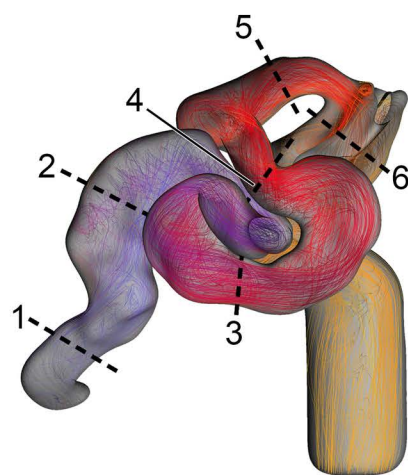
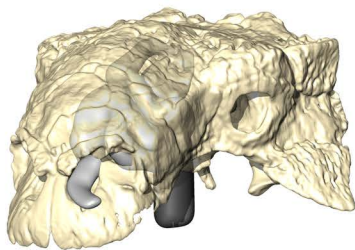
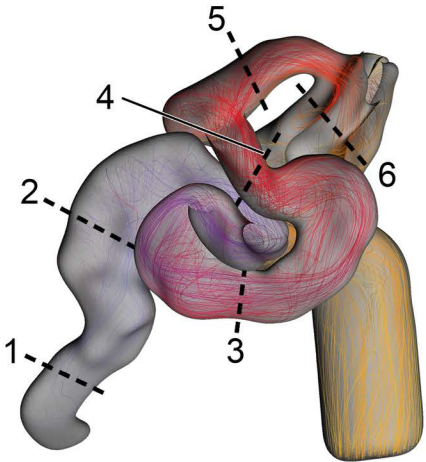
Low flow

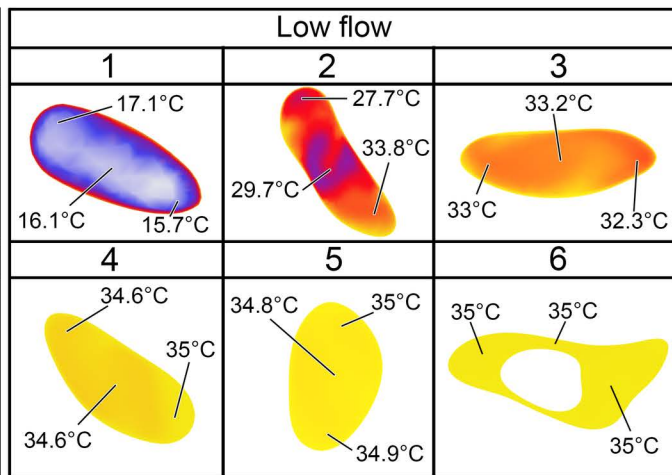
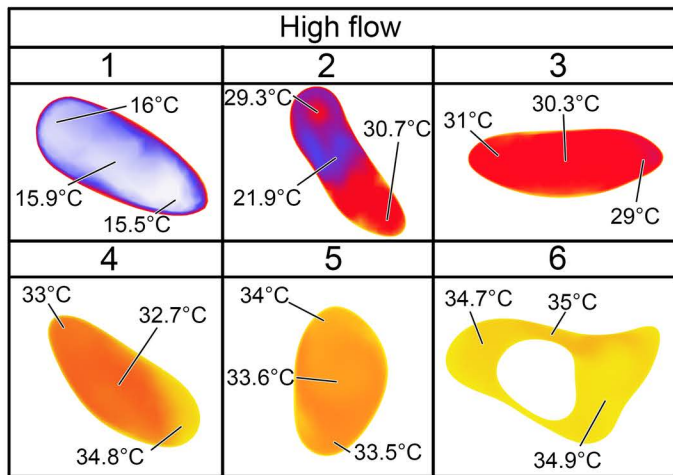
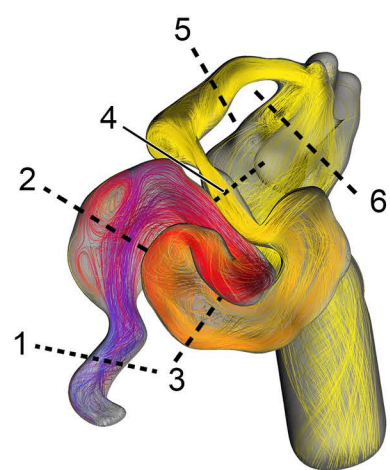
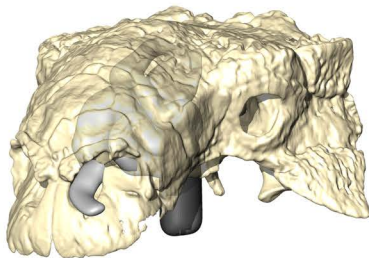
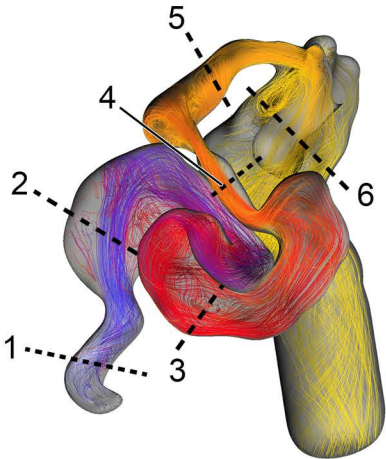


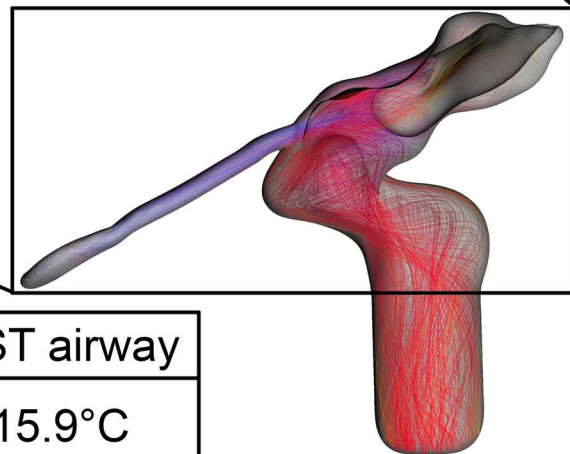
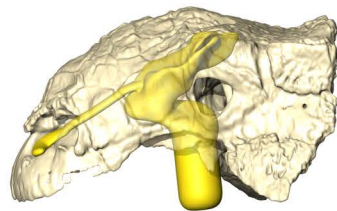
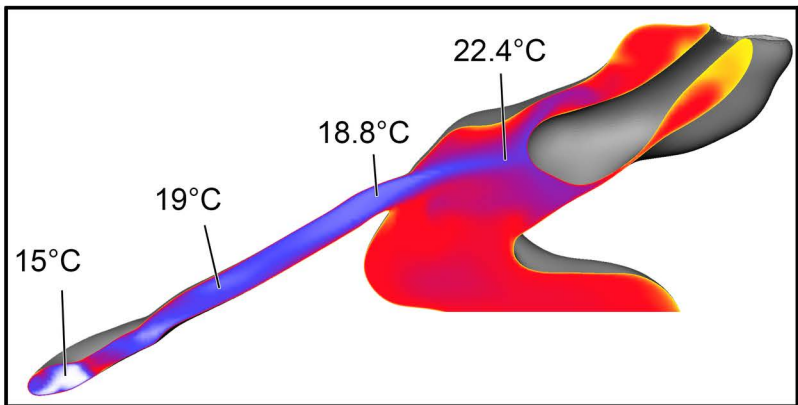
A**B**

	Basic airway	ST airway
Expired air temp	26.5°C	19.5°C

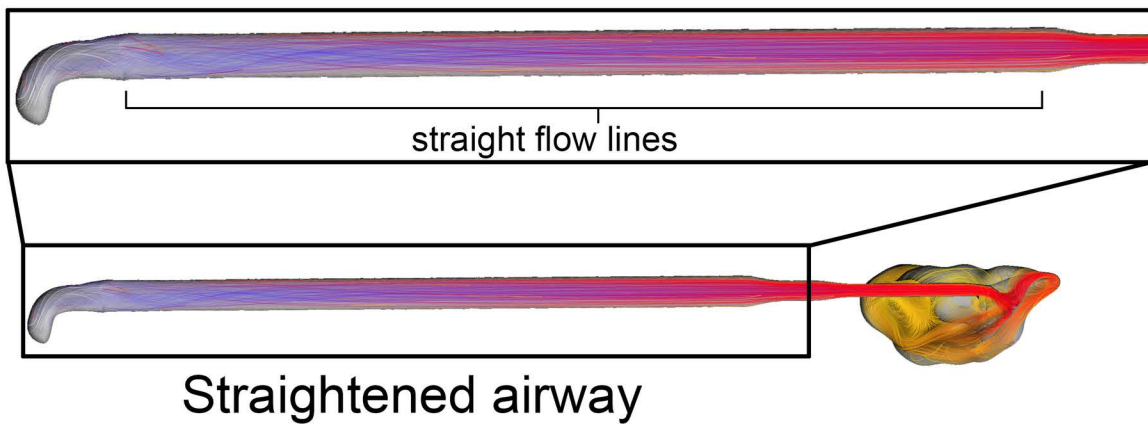
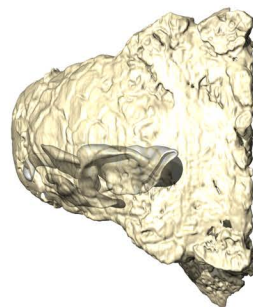
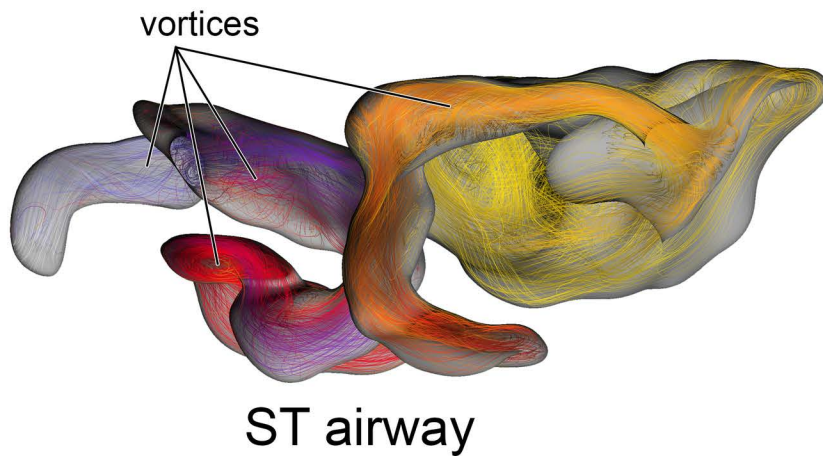


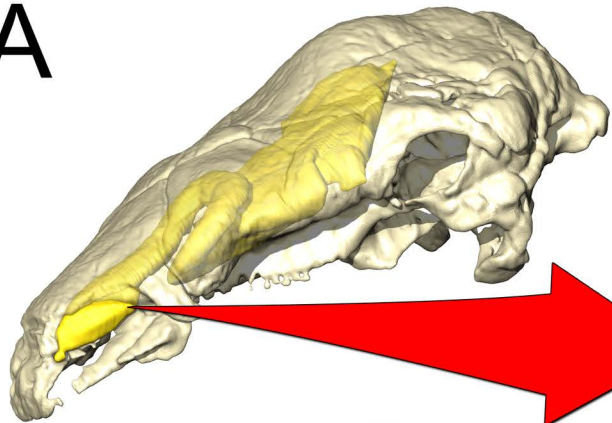
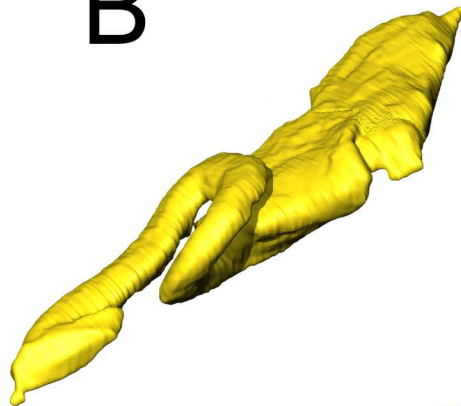
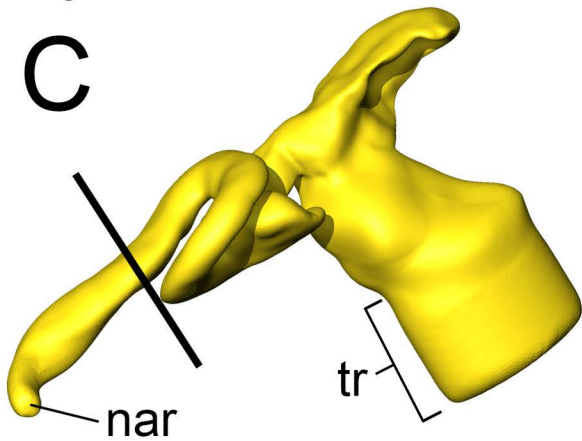
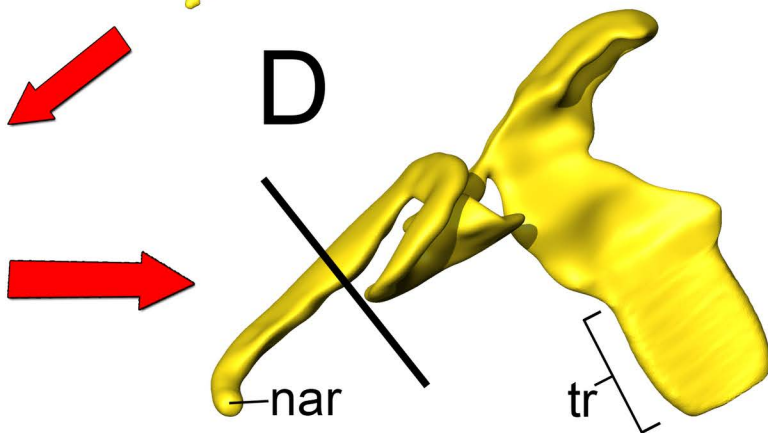
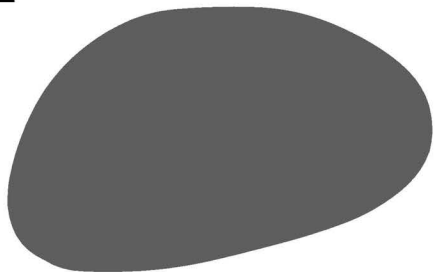




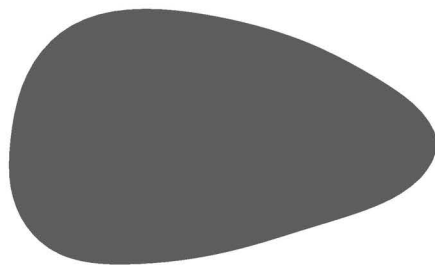
A**B**

	Basic airway	ST airway
Expired air temp	30.3°C	15.9°C

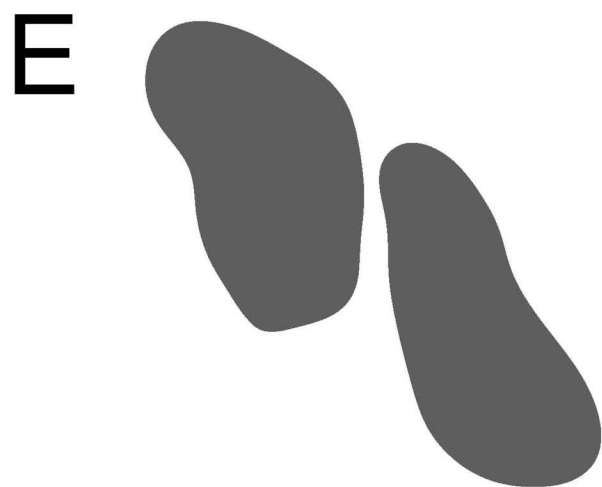
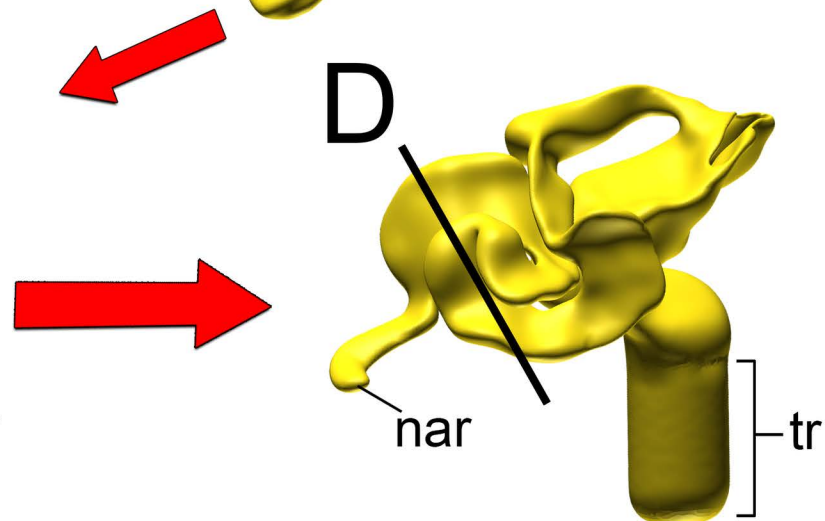
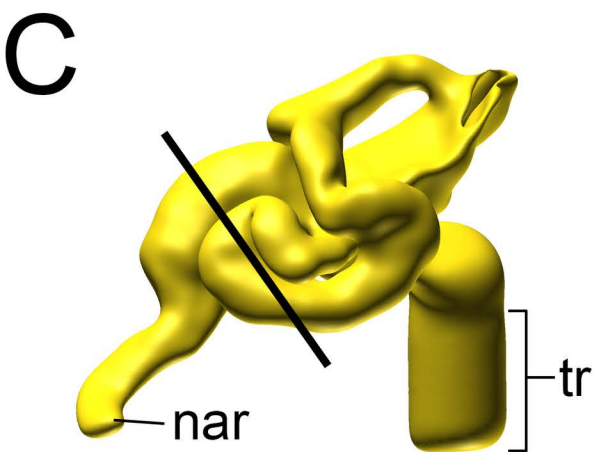
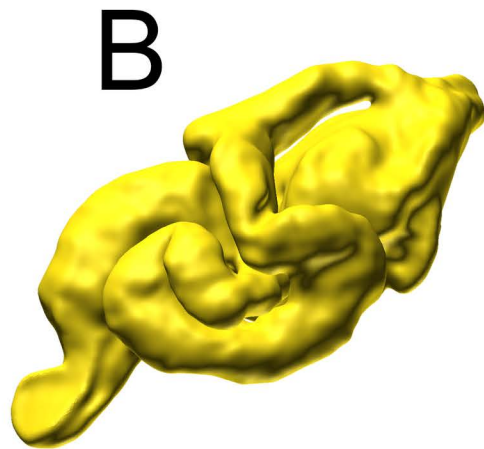
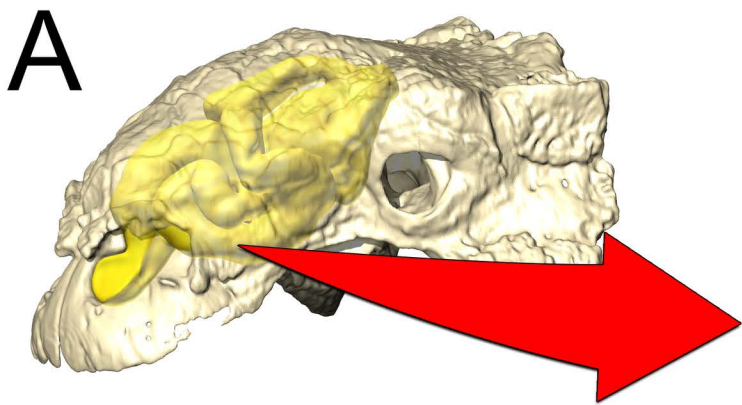
B**A****C**

A**B****C****D****E**

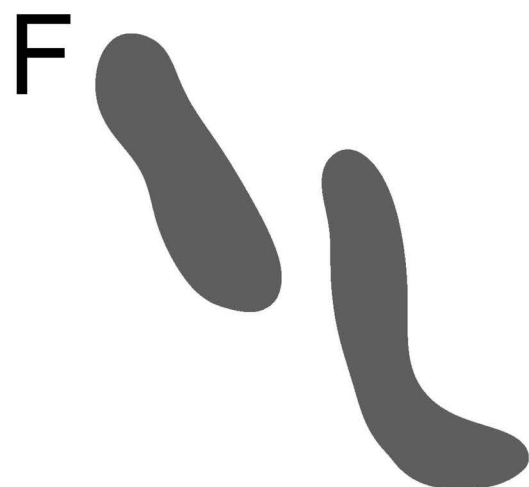
Avg: 17.4 mm

F

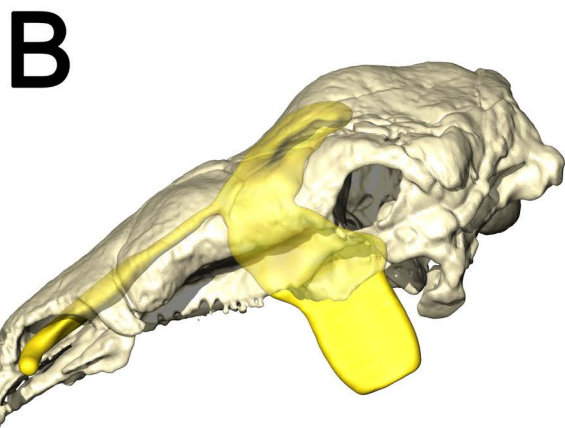
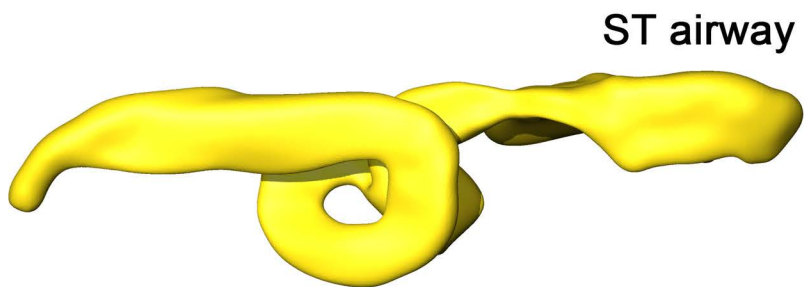
Avg: 10 mm



Avg: 22.8 mm

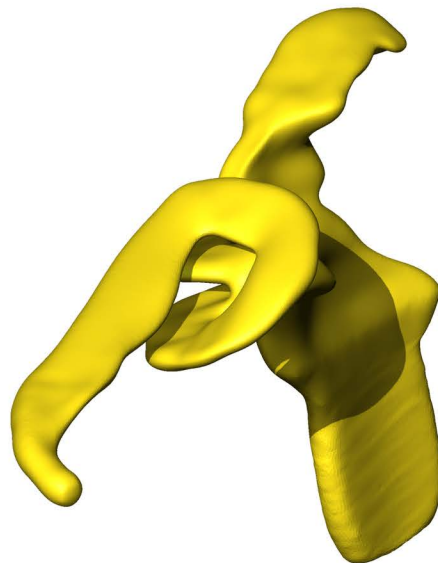
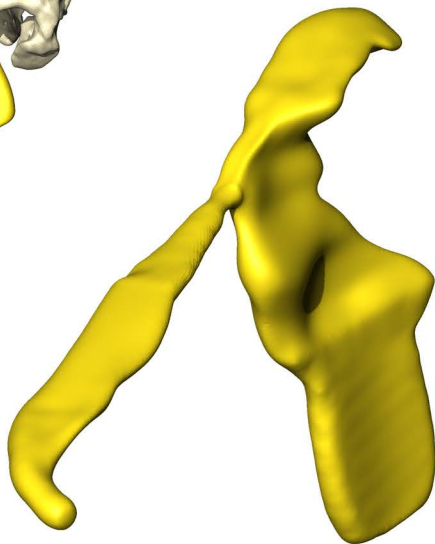


Avg: 10 mm



Basic airway

ST airway



vestibule length:

200 mm

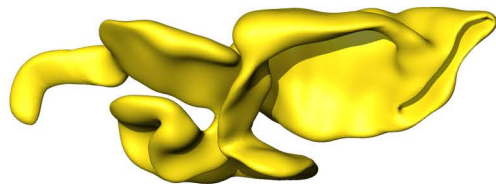
440 mm

A

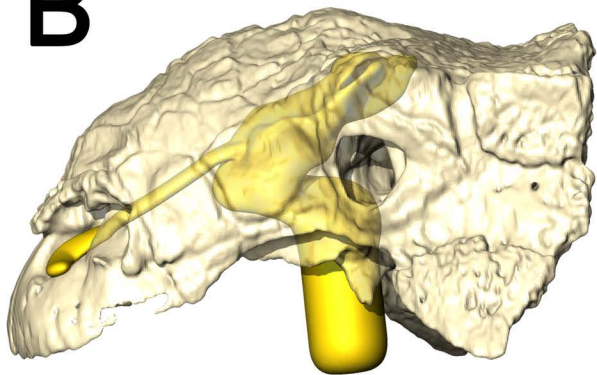
Straightened airway



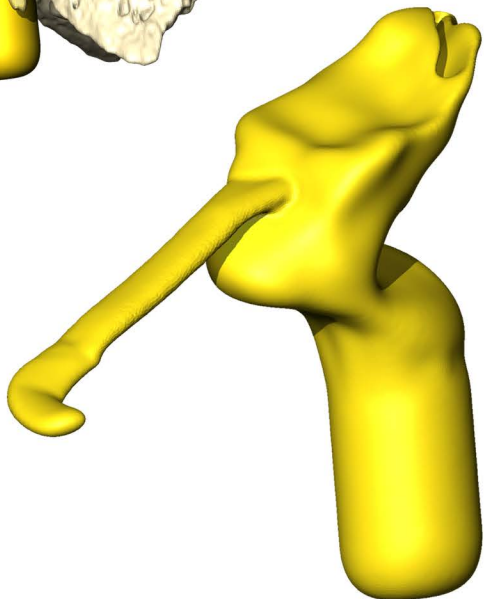
ST airway



B

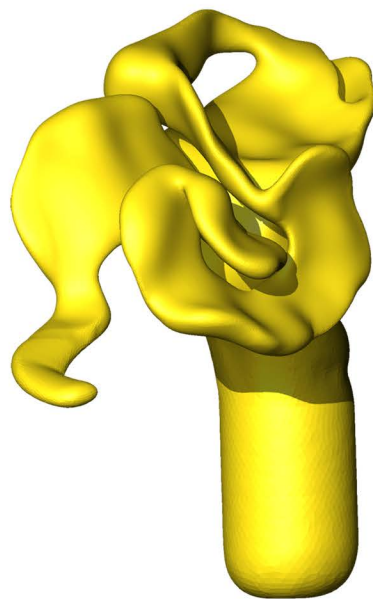


Basic airway



vestibule length: 162 mm

ST airway

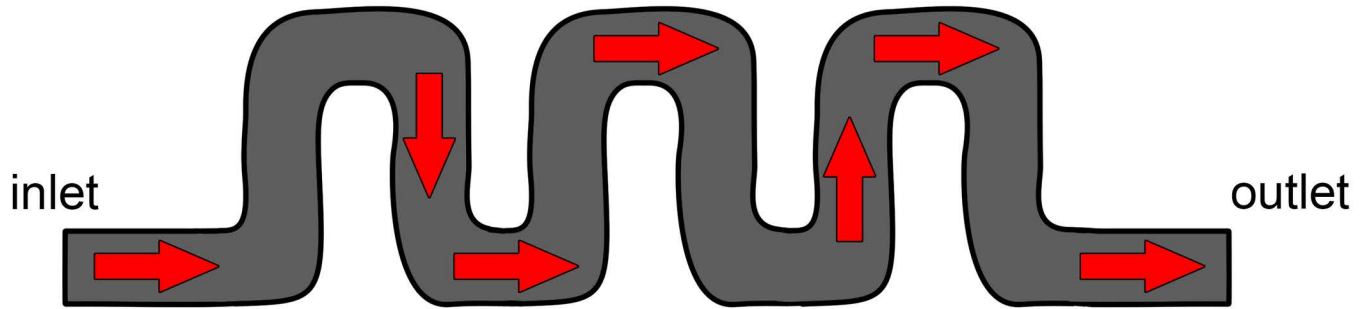


809 mm

serial flow

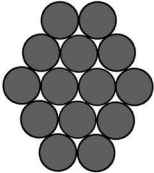
$$R = \frac{8\mu l}{\pi r^4}$$

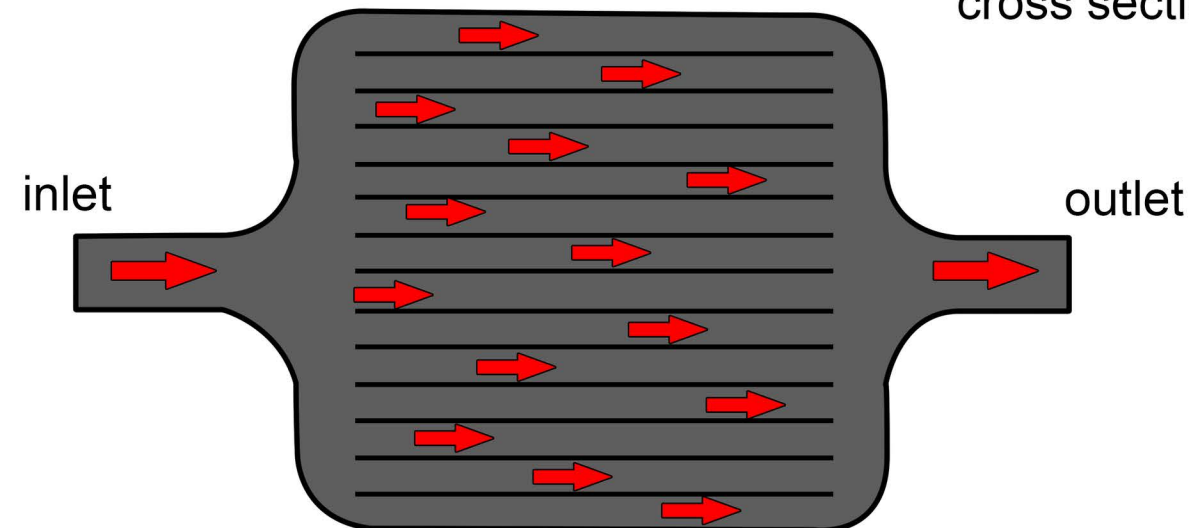
cross section: 



parallel flow

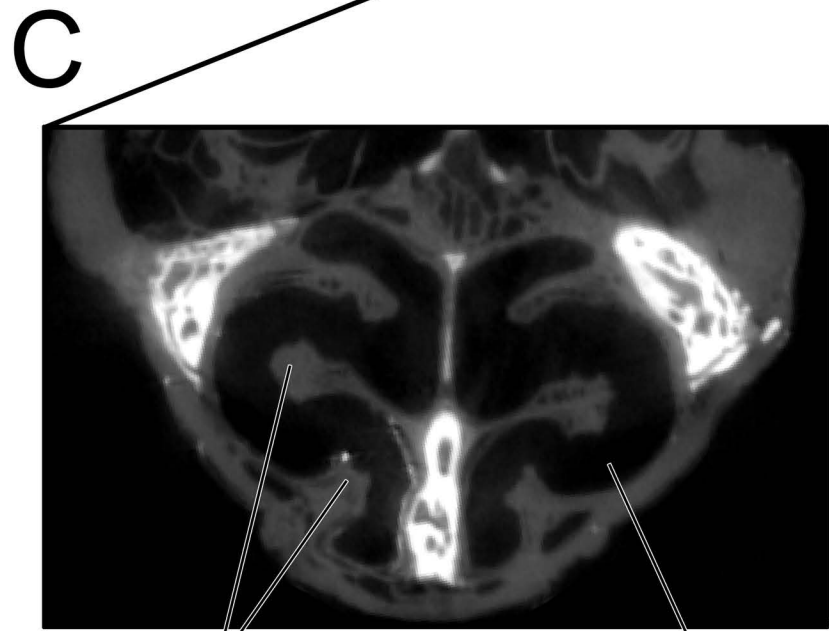
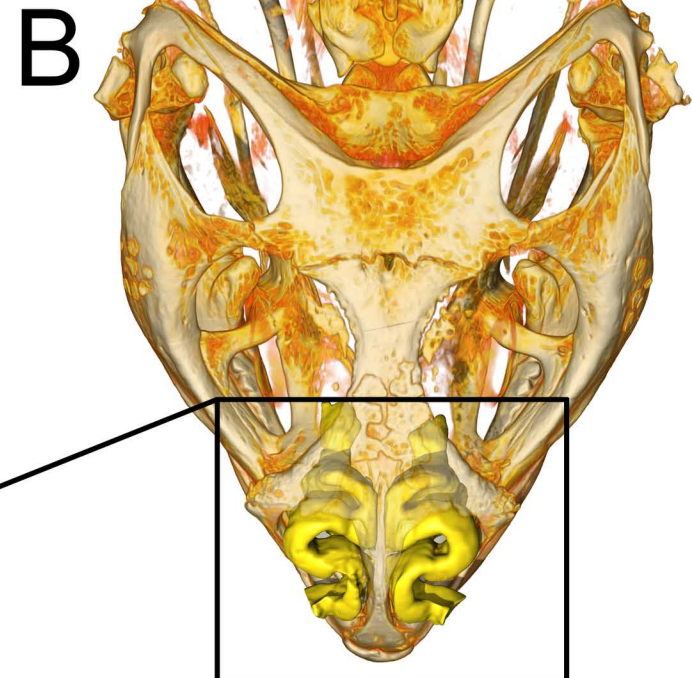
$$\frac{1}{R} = \sum \frac{1}{R} + \frac{1}{R} + \dots$$

cross section: 



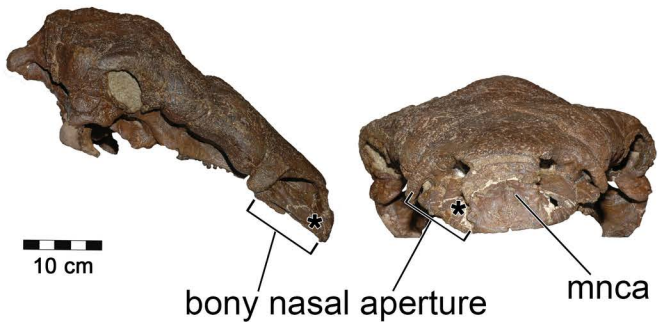
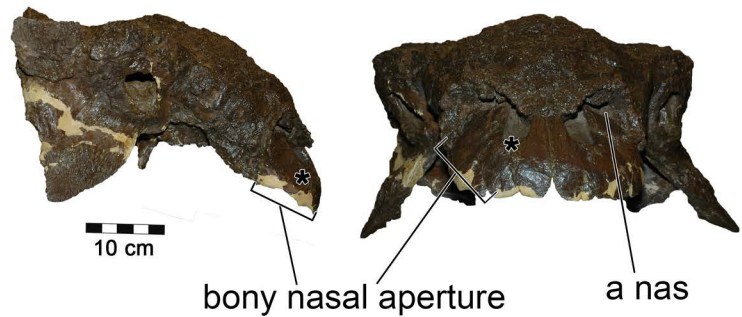
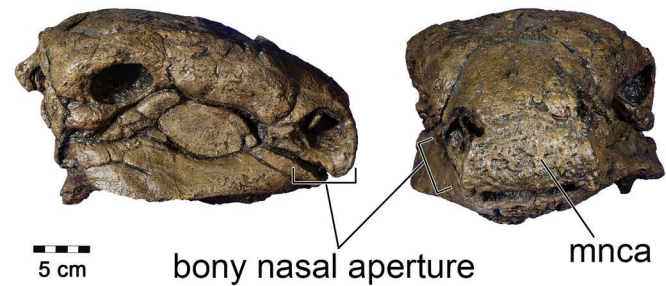
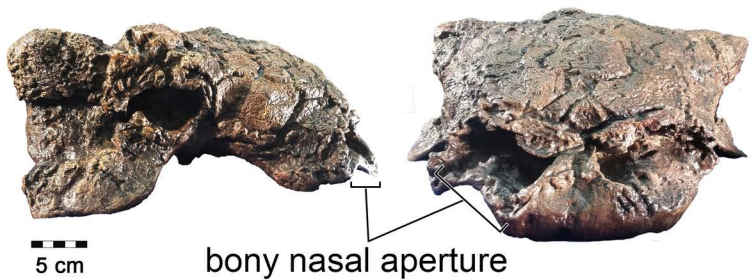


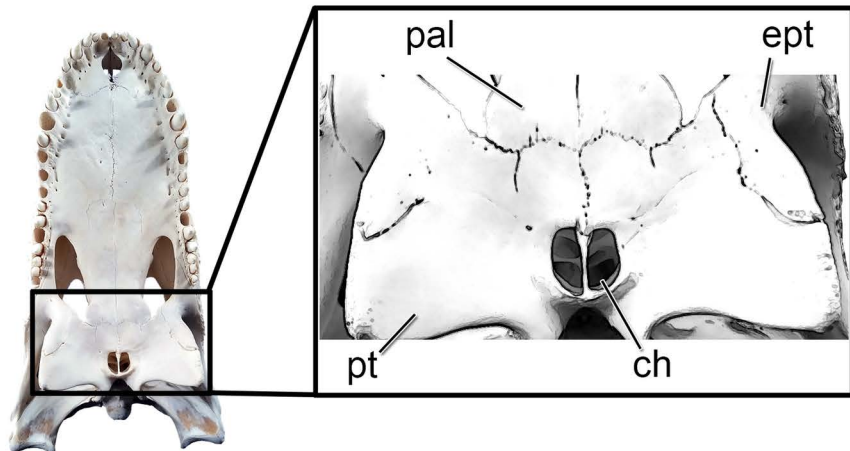
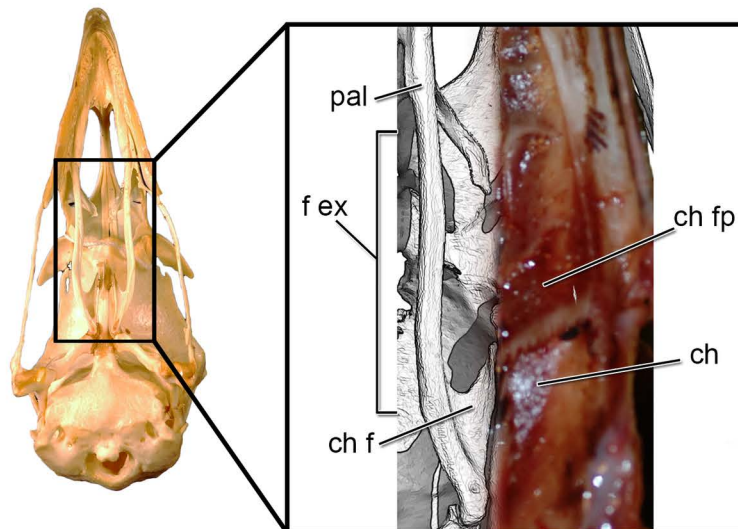
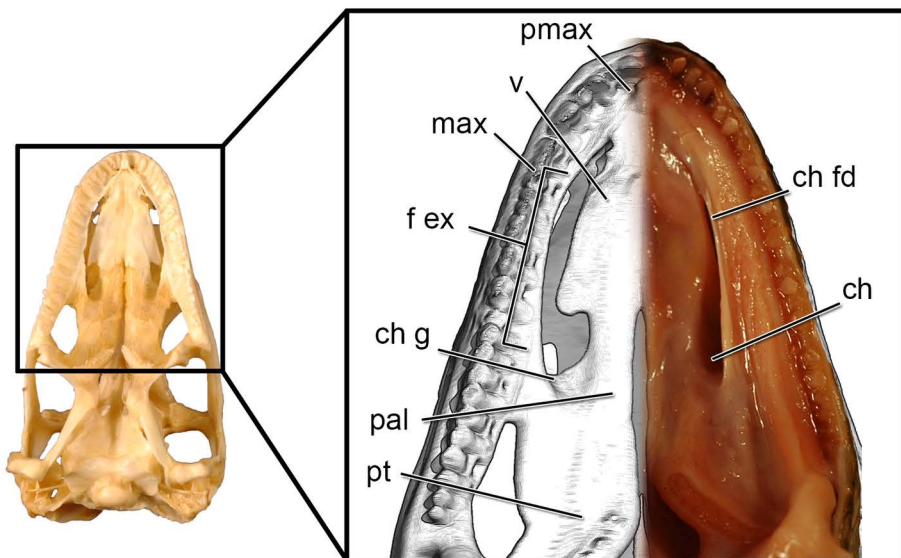
10 mm



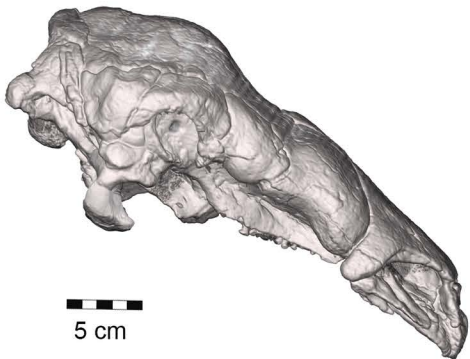
mucosa

airway

A**B****C****D**

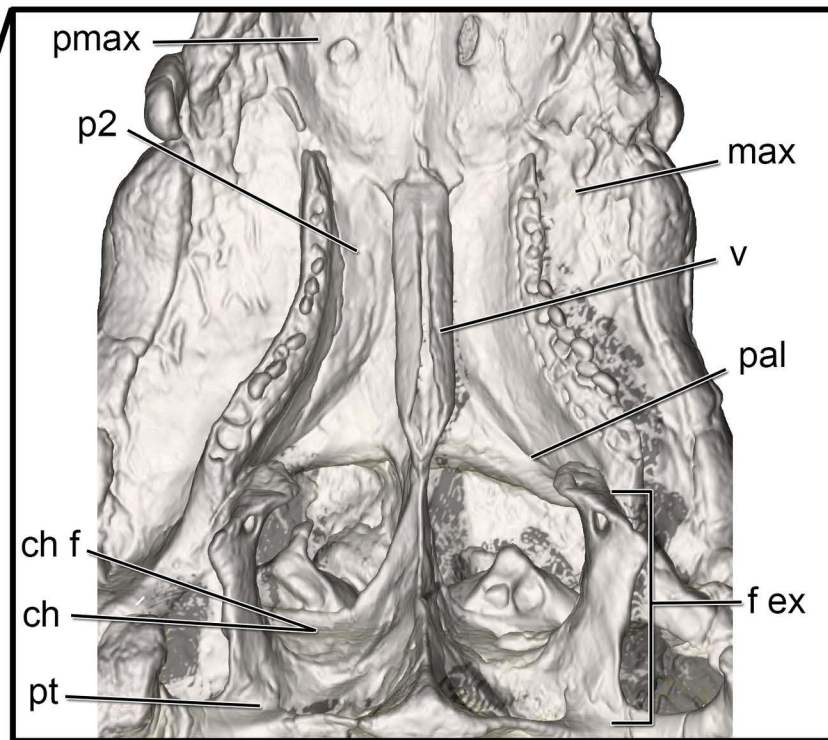
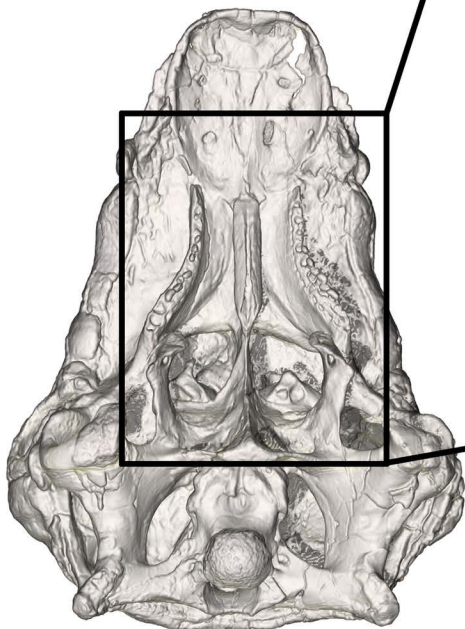
A**B****C**

A

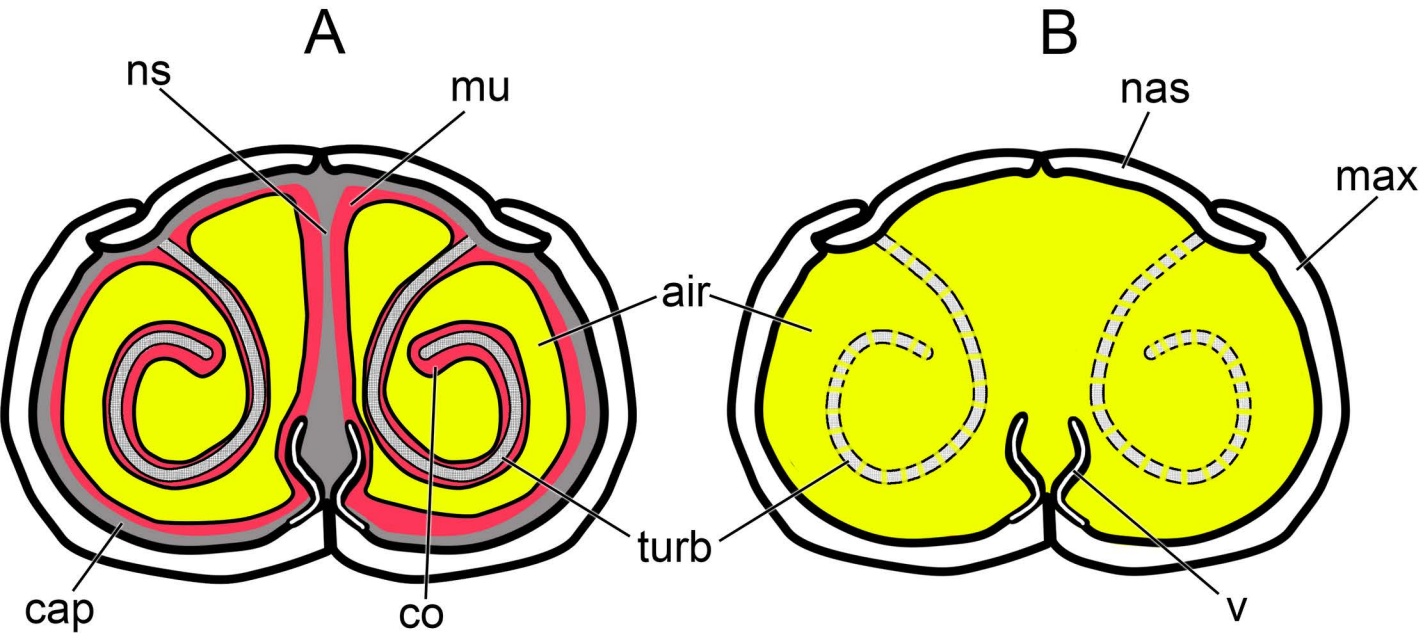


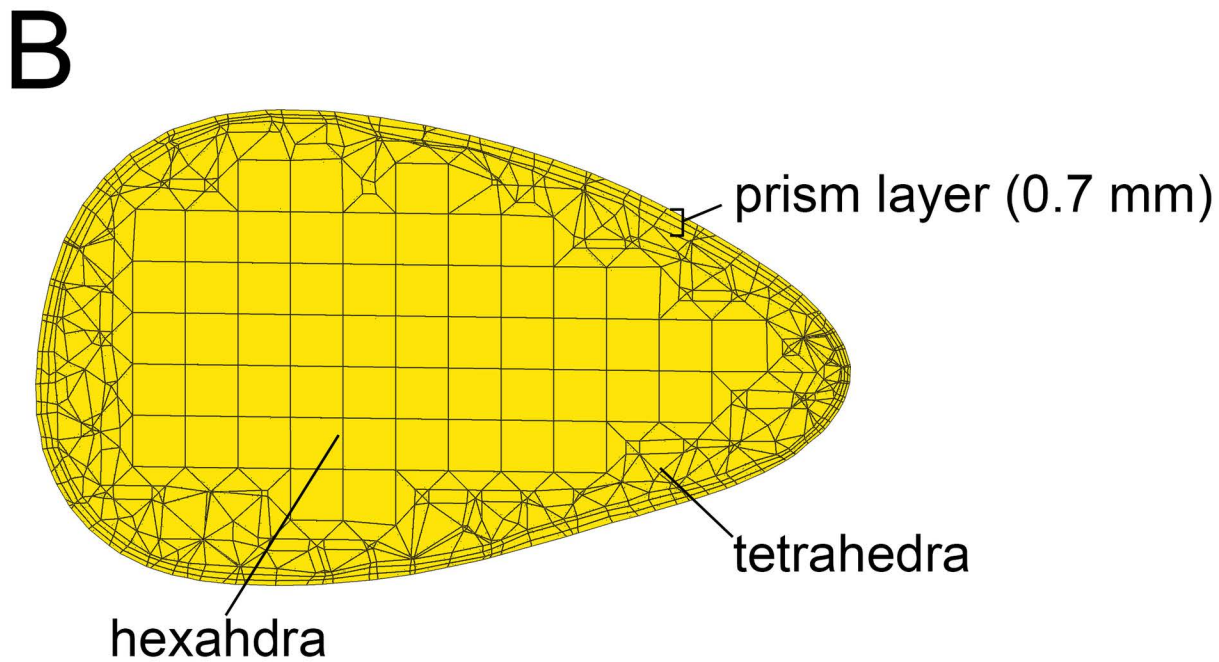
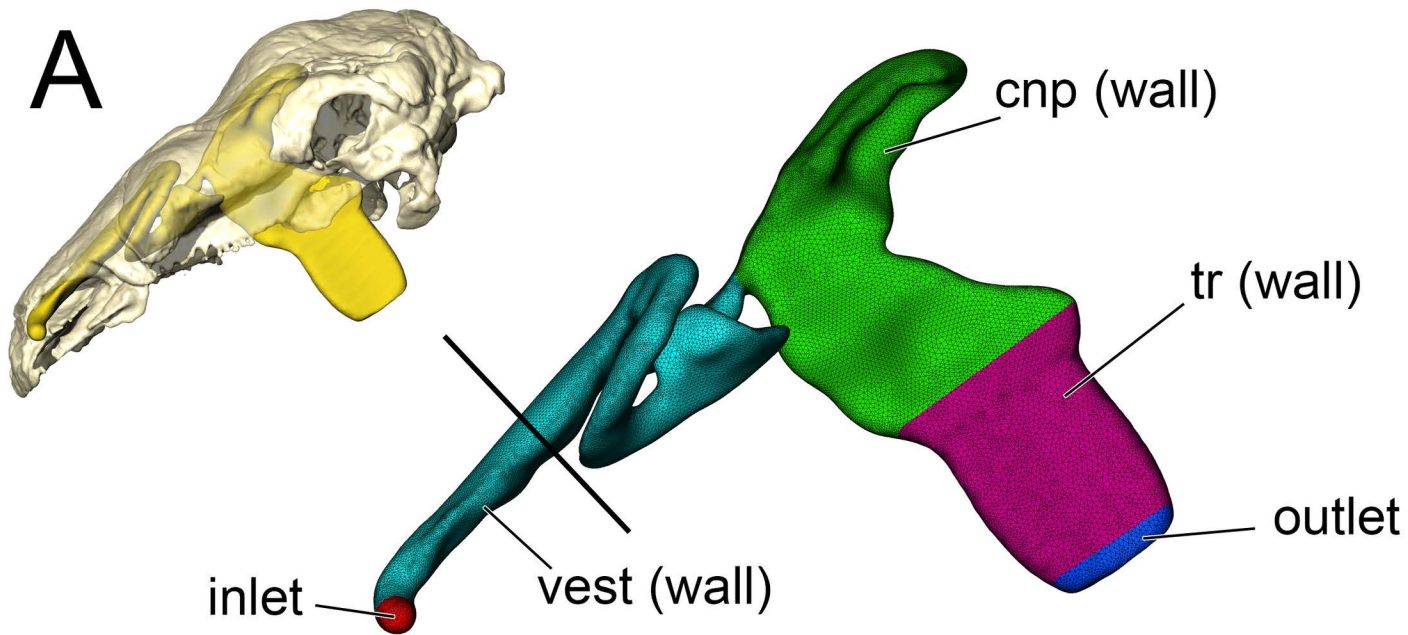
5 cm

B



5 cm





high resolution



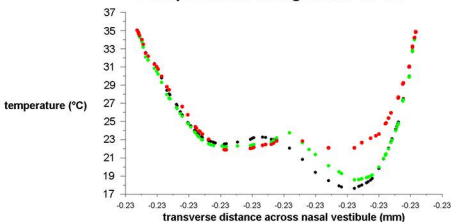
medium resolution



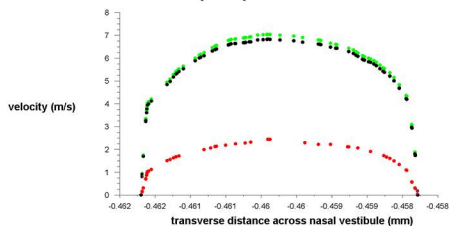
low resolution



Panoplosaurus straightened model

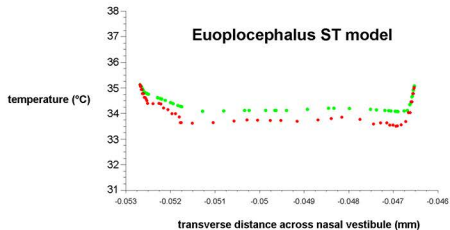


Euoplocephalus Basic model



model	<i>Panoplosaurus</i>	<i>Euoplocephalus</i>
bony-bounded (BB)	1,975,329	2,040,144
soft-tissue (ST)	3,518,193	1,341,829
basic	2,419,253	1,276,168
straightened	1,399,588	1,844,849

Euoplocephalus ST model



Panoplosaurus BB model

